Fransje Praagman & Femke Rambags

Migration of natural gas through the shallow subsurface

Implications on the surveillance of low pressure pipelines

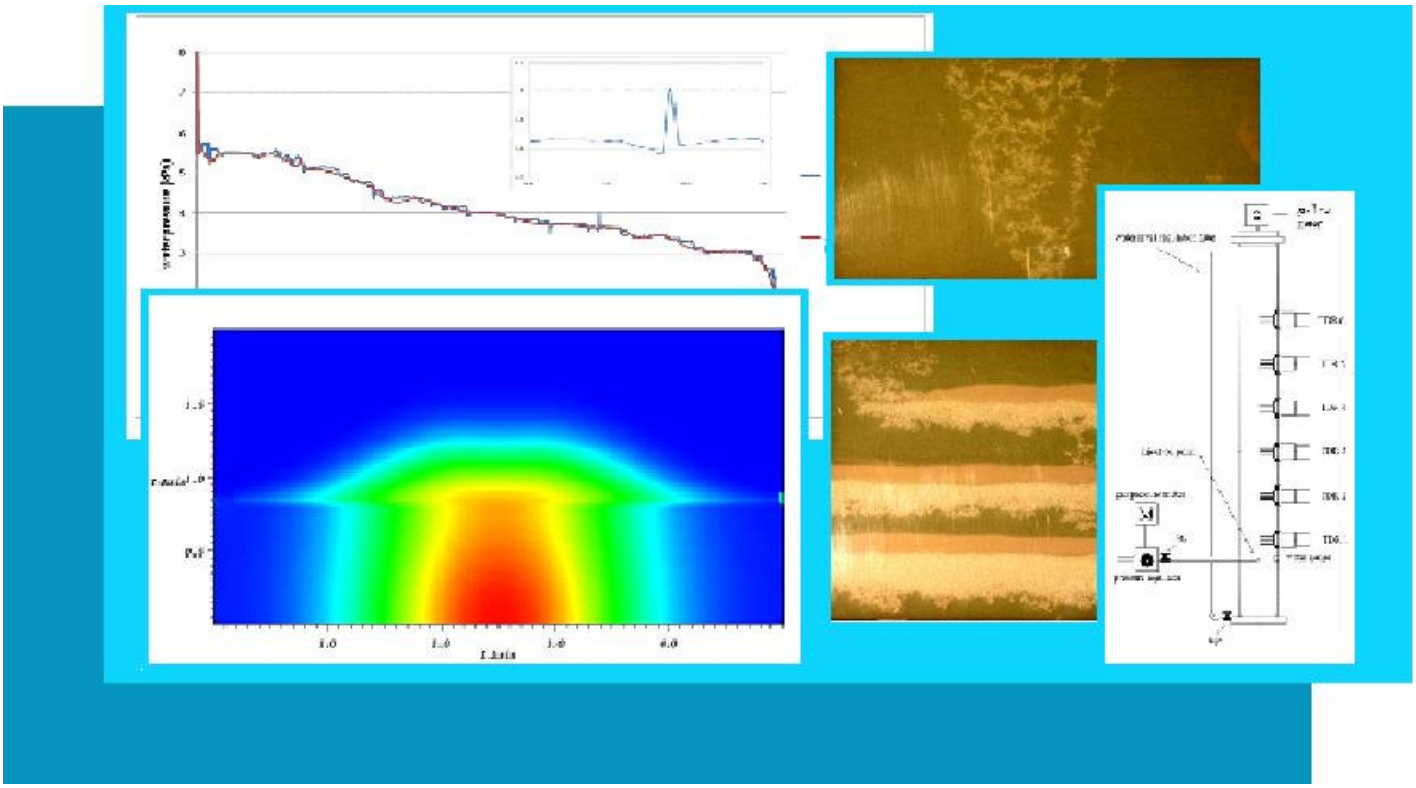

Universiteit Utrecht

Deltares
Enabling Delta Life

kiwa
Partner for progress

Migration of natural gas through the shallow subsurface

Implications on the surveillance of low pressure pipelines

A joint project of the University of Utrecht, Deltares and KIWA Gas Technology

MSc thesis submitted to the department of Earth Sciences 14-02-2008, University of Utrecht

Fransje Praagman & Femke Rambags

Supervisors:

Prof. dr. R. J. Schotting (University of Utrecht)
Dr. A. Bezuijen (Deltares)
Ir. V. van Beek (Deltares)
Drs. P. E. L. Schaminée (Deltares)
Dr. K. Pulles (KIWA Gas Technology)
Ir. Y. van der Drift (KIWA Gas Technology)

Abstract

Natural gas is a well known fossil fuel that is supplied to homes through low pressure pipelines. Because natural gas is a highly flammable gas mixture, a leakage in a pipeline can result in a serious safety hazard and it is essential to locate such a leakage as soon as possible. For this, knowledge of the processes that influence the flow of gas through the subsurface is necessary. The aim of this study is to get a better understanding of the flow of natural gas through the unsaturated zone from a leakage in a low pressure pipeline. Different parameters that influence the migration of gas, such as degree of saturation, pressure in the pipeline, grain size (distribution), are studied by conducting small-scale lab experiments and by numerical simulations using the multiphase flow program MUFTE-UG. Because of the complexity of the model, parallel computation is done at SARA, the most advanced computer and network center in the Netherlands.

Results indicate that the combination of different parameters determines the migration of gas through the subsurface. Increasing water saturation results in a decrease in spreading width and volumetric flux at the surface. An increase in gas pressure in the pipeline results in an increase of volumetric flux and spreading width. An increase in size of the leakage does not influence the spreading width of the gas, but does result in an increase in volumetric flux at the surface. It is important that layering of the soil or a low permeability layer on top of the soil is prevented when covering a pipeline. Layering results in an enhanced spreading width of the gas and makes it more difficult to locate the leakage. The use of a coarse sand with a small grain size distribution for the coverage of pipelines is recommended for a better detection of leakages.

Content

Notation of symbols

Symbol	*Definition*	*Dimension*
a	interfacial area per volume	[1/m]
A	surface area	[m^2]
bi	control volume or box for node i	[m^2,m^3]
$\|bi\|$	volume for the box associated with node i	[m^3]
C	concentration	[?]
$\mathbf{D}$	tensor of hydrodynamic dispersion	[m^2/s]
$\mathbf{D}^{K}_{m}$	molecular diffusion tensor of a component K in phase α	[m^2/s]
g	gravity	[m^2/s]
$\mathbf{g}$	vector of gravitational acceleration $(0,0,-g)T$	[m⁄s^2]
h	piezometric head	[m]
K	hydraulic conductivity	[m⁄s]
kr	relative permeability	[-]
L	length	[m]
$\mathbf{n}$	outer normal vector	[-]
n	Van Genuchten (VG) parameter	[-]
N_i	ansatz functions functions for node i	[-]
P	pressure	[Pa]
P_c	capillary pressure	[Pa]
P_d	entry pressure for the Pc(Sw) relationship after Brooks & Corey	[Pa]
q	scalar Darcy velocity	[m⁄s]
$\boldsymbol{q}$	tensor Darcy velocity	[m/s]
Q	volumetric flux	[m3⁄s]
R	radius	[m]
R_e	Reynolds number	[-]
S	saturation	[-]
$S_{r\alpha}$	residual saturation of phase α	[-]
S_e	effective saturation of the wetting phase	[-]
t	time	[s]
T	temperature	[K]
V	volume	[m3]
V_f	volume fraction	[-]
W_i	weighting function for node i	[-]
z	elevation head	[m]
α	Van Genuchten (VG) parameter	[Pa^{-1}]
κ	intrinsic permeability	[m2]
λ	mobility	[-]
μ	dynamic viscosity	[kg/(ms)]
σ	surface tension	[N/m^2]
$\Psi_{\alpha i}$	total potential of phase α at node i	[-]

Subscripts:

α	phase, either wetting (w) or non-wetting (n)

n	non-wetting phase
f	pore
g	gas phase
s	solid phase
t	total
w	wetting phase

1. Introduction

1.1 Motivation

Natural gas is a well known fossil fuel that is supplied to homes, where it is used for such purposes as cooking and central heating. On average a Dutch household uses approximately 1600 m^3 of natural gas per year. Before natural gas reaches a household it has to be produced from gas fields and converted into natural gas which mainly consists of methane. The major difficulty in the use of natural gas is transportation to these households because of the low density of the gas. To make transport possible natural gas is first compressed and transported through high pressure gas pipelines and later decompressed and transported through low pressure pipelines which supply the gas to houses. In the Netherlands there are approximately 100.000 km of low pressure gas pipes. The surveillance and maintenance of this pipe network is the responsibility of network managers. Because natural gas is a highly flammable gas mixture surveillance and maintenance of pipelines is of great significance. If a leakage may occur in a distribution pipe it is essential to locate this leakage as soon as possible.

Experience has shown that high gas concentrations are not necessarily measured in close proximity of a leakage, but can be observed more than 10 m from the exact location of a leakage. To be able to determine the correct location of a leakage it is important to understand how natural gas will spread in the subsurface. This knowledge will have practical implications on the surveillance, maintenance and safety of transport of natural gas in the subsurface.

To obtain knowledge about the spreading of natural gas in the Dutch subsurface a research project is defined by KIWA Gas Technology together with the University of Utrecht and Deltares. It is funded by Enbin. The general aim of this study is to model the flow of gas in unsaturated Dutch soil from a leakage in a low pressure distribution pipe. The results of this research will be used to adress practical questions of the network managers on the flow of natural gas in the subsurface. These will later be translated into adjustments of procedures, guidelines and work instructions for the detection of natural gas in the field.

1.2 Previous work and problem description

Gas distribution pipelines in the Netherlands are generally located in unsaturated soils. When there is a leakage in a distribution pipe gas will thus flow through a porous media that is partially saturated with water. A short literature study shows that at this moment not much is known about the flow of natural gas in the unsaturated subsurface.
Some large scale experiments simulating a gas pipe leakage were conducted by Brötzenberger and Pass (1987). They concluded that the flow of gas in the subsurface is strongly dependent on degree of saturation of the soil. In this particular study only experiments were conducted and no link with any type of theoretical model was made, which makes it hard to translate the results to other situations. Such a theoretical model for the flow of gas through the subsurface

was constructed by Iwata, Hamaide and Fuchimoto (1992). This model is a one-phase flow model based on Darcy's law. Because flow of gas through the unsaturated zone is a clear example of a two-phase flow problem this model is too simple to apply to the flow of gas in unsaturated Dutch soils. More extensive numerical research has been done on the migration of gas through the unsaturated zone from waste disposal sites (Dogan, 2004, Metcalfe & Farquhar, 1987). Although they are based on the same theories, the scale and time span of the simulations are very large compared to problem of gas flowing from a leakage.
Another important aspect that is not covered by the above discussed studies is the influence of natural soil variability on the flow of gas. Delahey and Alonso (2002) explored this effects using a multiphase flow model. Their results indicated that natural soil heterogeneity can cause gas flow to be concentrated around some preferential path.

From literature it can thus be concluded that soil heterogeneity and saturation of the soil have a significant influence on the flow of gas. This information alone is not enough to accurately and quantitatively describe the flow of gas through the unsaturated zone. More insight on the influence of grain size distribution and degree of saturation that are common for Dutch soils is needed. Moreover the depth and size of the leakage and the pressure in the pipeline should be taken into account.

1.3 Goals and structure

The goal of this research is to model the flow of gas from a leakage in a low pressure distribution pipe through the unsaturated Dutch soil. This very broad question is divided into a number of particular research questions:

- How does the degree of saturation influence the flow of gas through the unsaturated zone?
- What is the influence of grain size (distribution) and soil heterogeneity on the flow of gas?
- What is the influence of pressure variations in the pipelines?
- What is the effect of precipitation?

These phenomena must be studied to get an impression of the minimum and maximum spreading width of the gas and the variation in volumetric fluxes measurements at the surface for different soil types and degrees of saturation.

To answer these research questions and accurately describe the flow of natural gas through the unsaturated Dutch subsurface both numerical and experimental research are conducted. For the numerical simulation of the multiphase flow and transport computer code MUFTE-UG is used. This code is constructed by the University of Stuttgart in cooperation with the University of Heidelberg. Simultaneously small scale experiments are conducted to gain more insight in the problem and verify the outcomes of the numerical study.

This thesis has the following structure. First the theoretical considerations for the concept of two-phase flow in a porous media will be given in Chapter 2. The mathematical model that is derived from this theory, which is the basis of the numerical code, will be described in Chapter 3. In Chapter 4 the multiphase flow model MUFTE-UG is described and an explanation of the numerical discretization methods is given. A description of the different simulations and results are given in Chapter 5. The laboratory experiments are described and discussed in Chapter 6. In Chapter 7 numerical and experimental results are compared and discussed. Moreover we attempt to translate the results into possible implications on the surveillance, maintenance and safety of transport of natural gas in the subsurface. Recommendations for further research are discussed in this chapter. Finally a short summary is given and conclusions are drawn in Chapter 8.

2. Theoretical considerations

The flow of gas through the unsaturated zone is a typical example of two-phase flow, which is the simultaneous flow of two immiscible fluids or phases through a porous medium. Immiscible fluids are fluids that share a distinct fluid-fluid interface and cannot be mixed. In addition to the immiscible fluids there is also a solid phase, which is the porous medium. Depending on the wetting properties of the fluids, one of the two immiscible fluids will be a wetting and the other a non-wetting fluid.
Two-phase flow is a frequently studied subject in chemical engineering, hydrology, and reservoir engineering, but in most cases the flow of the liquid is studied, whereas in this study the emphasis is on the flow of the gas phase. In the case of two-phase flow, the permeability of the porous medium depends on grain size and degree of saturation. In case of a saturated soil, gas can only flow by removing water from the pores. The ability to remove water from the pores is dependent on pore size. Water has the tendency to stick to the grains, which makes it harder to remove water from smaller pores. This phenomenon is called capillary pressure, which can be defined as the difference in pressure across the interface of two immiscible fluids.
Capillary pressure depends on grain size, and will be higher for smaller grains. Gas can only remove water from the pores if the gas pressure exceeds the capillary pressure. Entry pressure is defined as the minimum gas pressure needed to remove water from the pores. If the entry pressure is larger than the gas pressure, the porous medium will be impermeable for gas.

In this Chapter the governing equations of two-phase flow are given. Because permeability is strongly dependent on saturation and grain size, two-phase flow in unsaturated porous media is a highly non-linear process, which is very sensitive to details. These non-linear equations can only be solved analytically for very simple cases. Therefore, the complex system of equations is approximated using numerical methods. This is further explained in chapters 4 and 5.

2.1 Preliminary remarks

When modeling two-phase flow it is important to consider at what scale the flow is modeled. At the micro (i.e. pore) scale a mathematical point within one phase or at the interface between phases is considered. At this scale discontinuities, which are small compared to the pore or grain diameter, can be clearly recognized and the investigated phases are separated from each other. When looking at a macroscopic scale the properties at the micro scale are averaged within a representative elementary volume (REV) (Figure 2.1). This requires a macroscopic continuum where discontinuities that can be recognized at the micro scale can no longer be identified.

In modeling, the transition from the micro to the macro scale is important to consider, because equations that describe fluid-fluid interfaces and flow at the microscale can not automatically

be applied to the macro scale. This is only possible if the characteristic properties of the flow and transport processes at the micro scale can be attributed to the flow and transport processes at the macro scale. If so, a careful averaging process can be applied to transform micro scale equations to equations that are valid at the macro scale.

A scale transition is closely related to the concept of the Representative Elementary Volume (REV) after Bear, 1972. A REV is a volume over which one has to average a porous medium property such that it no longer depends on pore-scale fluctuations. It is assumed that the fluctuations of an averaged parameter are negligible for a length *l*, with $d << l << L$, where *d* represents a length scale of the pore scale and *L* represents a larger scale where again fluctuations in the averaged parameter might occur due to heterogeneities (Helmig, 1997).
Over the length *l* the average of the variable considered does not change with an altering averaging volume.

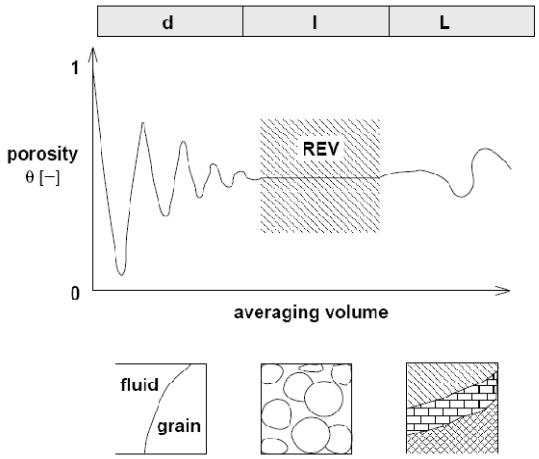

Figure 2.1 concept of Representative Elementary Volume (REV). Taken from Helmig, 1997.

2.2 Phase properties

At the micro scale, a phase is interpreted as a substance with a certain volume separated by interfaces from other phases. At the macro scale it is no longer possible to distinguish between different phases and only the volumetric ratio between phases can be described.

A porous medium is a solid phase that has void spaces. The void space in the porous medium is defined by the porosity, which is the volume of pores with respect to the total volume of the porous media:

$$\phi = \frac{V_f}{V_t}, \tag{2.1}$$

where ϕ is the porosity, V_f is the volume of the pores, and V_t is the total volume of the porous medium.
In these pores fluids can be present. Fluid flow can only occur in interconnected pores. Effective porosity is defined as the volume of interconnected pores with respect to the total volume of the porous media.

$$\phi_{effective} = \frac{V_f^{\text{int}\,erconnectad}}{V_t} \quad , \tag{2.2}$$

where $\phi_{effective}$ is the effective porosity and $V_f^{\text{int}\,erconnected}$ is the volume of interconnected pores. The pore space can be occupied by one or more fluids. The porosity of a soil depends on its texture and is only a measure of the total volume of the pores, not of the pore size and usually varies between 0.35 and 0.5.

2.3 Conservation equations

2.3.1 One-phase flow

When there is only one phase present in a porous medium (e.g. the liquid phase), flow through the soil is called one-phase flow. At the macro scale the flow of a one-phase fluid in an isotropic medium can then be described using the empirically derived Darcy equation (Hillel, 1997):

$$q = K\frac{\Delta H}{L} \quad , \tag{2.3}$$

where q is the flux density, which is the amount of water flowing through a cross-sectional area per unit time, K is the hydraulic conductivity, ΔH is the hydraulic head difference and L is the length of a soil column.

In one dimension, Darcy's law can be written in differential form, yielding:

$$q_x = -K\frac{dH}{dx} \, , \tag{2.4}$$

where q_x is the specific discharge in the x direction.
Alternatively, the hydraulic head can be expressed in terms of pressure, which yields the following equation (Fitts, 2002)

$$q_x = -K\frac{d}{dx}\left(\frac{P}{\rho g}\right) = -\frac{K}{\rho g}\frac{dP}{dx} = -\frac{\kappa}{\mu}\frac{dP}{dx} \, , \tag{2.5a}$$

where the definition of hydraulic conductivity is used:

$$K = \frac{\kappa \rho g}{\mu} \tag{2.5b}$$

where P is pressure, ρ is the density of the fluid, g is the gravitational acceleration, κ is the intrinsic permeability, and μ is the dynamic viscosity. The dynamic viscosity is a

proportionality factor which is primarily determined by the temperature T and the components dissolved in water (Helmig, 2007). In equation (2.5a) pressure is the driving force and viscous forces constitute the resistive forces.

In three dimensions, with gravity taken into account, the equation becomes:

$$\mathbf{q} = \frac{-\boldsymbol{\kappa}}{\mu}(\nabla P - \rho \mathbf{g}) \tag{2.6}$$

To correctly describe unsteady flow processes, in which the direction and magnitude of flow change with time, Darcy's law should be used in combination with the law of conservation of mass. This law states that if more mass is flowing into a reference volume than there is flowing out, the difference in mass should be inside the reference volume. This leads to the following equation:

$$\frac{\partial C}{\partial t} + \nabla \cdot \rho \mathbf{q} = 0 \tag{2.7a}$$

$$C = \phi S \rho \tag{2.7b}$$

where S is the water saturation.

Substituting Darcy's law and equation (2.7b) in equation (2.7a) gives:

$$\frac{\partial(\phi S \rho)}{\partial t} - \nabla \cdot \left(\rho \frac{\boldsymbol{\kappa}}{\mu} (\nabla P - \rho \mathbf{g}) \right) = 0 \tag{2.8}$$

When there are sources and sinks present in the reference volume, a term should be added to account for them, since they also affect the amount of water in the volume. In the case of one-phase flow, $S = 1$, and thus constant in time. Assuming a constant porosity in time, this leads to the final conservation equation:

$$\phi S \frac{\partial \rho}{\partial t} - \nabla \cdot \left(\rho \frac{\boldsymbol{\kappa}}{\mu} (\nabla P - \rho \mathbf{g}) \right) - \rho q_s = 0 \tag{2.9}$$

Where q_s is secondary volume flux in $m^3/(m^3 s)$ which is the term for the sources and sinks.

2.3.2 Multiphase flow

In the case of multiphase flow, the conservation equation is extended for multiple phases, where the subscript α denotes the different phases. Assuming a constant porosity in time, the conservation equation becomes:

$$\phi S_\alpha \frac{\partial \rho_\alpha}{\partial t} + \phi \rho_\alpha \frac{\partial S_\alpha}{\partial t} - \nabla \cdot \left(\rho_\alpha \lambda_\alpha \mathbf{\kappa} \left(\nabla P_\alpha - \rho_\alpha \mathbf{g}\right)\right) - \rho_\alpha q_\alpha = 0 \qquad (2.10)$$

where

$$\lambda_\alpha = \frac{k_{r\alpha}}{\mu_\alpha} = \text{mobility of phase } \alpha \qquad (2.11)$$

Here, the relative permeability ($k_{r\alpha}$) is introduced as a scaling factor, to account for the influence of other phases on the flow of one phase.

Diffusion

There is also a non-convective mass flow $\boldsymbol{w}$ caused by molecular diffusion which should be added to the mass conservation given above. This can be described by Fick's law of diffusion (Helmig, 1997):

$$\boldsymbol{w} = -\phi \boldsymbol{D}^c_{m,pm} \nabla (\rho_{mol,\alpha} X^c_\alpha) \qquad (2.12)$$

Where $\boldsymbol{D}_{m,pm}$ is the tensor of molecular diffusion which can be assumed to be homogeneous and isotropic. $\boldsymbol{D}_{m,pm}$ is strongly dependent on material properties and must be defined for each component c. Diffusion is often negligible compared to convection.

Mechanical dispersion

As a result of micro scale velocity profiles in pore channels, by splitting of flow paths through the pore network or as a results of macroscopic soil heterogeneities spatial fluctuations in velocity can occur. In an REV there are fluctuations in the distribution of the velocity in space and time. These fluctuations refer to the size and orientation of the velocity vector. They are taken into account by the concept of mechanical dispersion. Mechanical dispersion is proportional to the magnitude of the average velocity. For an isotropic medium with an arbitrary orientation of the velocity vector in space, the dispersion tensor $D_{d,pm,ij}$ can be written as;

$$D^c_{d,pm,ij} = \alpha_T \delta_{ij} \boldsymbol{v} + (\alpha_L - \alpha_T) \frac{\boldsymbol{v}_i \boldsymbol{v}_j}{\boldsymbol{v}} \qquad \text{Bear (1979)} \qquad (2.13)$$

Where α_T is the transversal dispersivity, α_L is the longitudinal dispersivity, δ_{ij} is the Kronecker delta and $\boldsymbol{v}$ is the velocity vector.

Because the mathematical description of diffusion and dispersion are very similar, they are often combined in one tensor $\boldsymbol{D}_{pm}$ which can be defined for every component.

2.4. Capillary pressure

When two immiscible phases are in contact, their interface will be curved due to pressure differences between the wetting and the non-wetting fluid. This pressure difference is called capillary pressure. The wetting fluid is the fluid with the strongest molecular attraction, and as a result will form the coating of the solid surfaces, whereas the nonwetting fluid will occupy the central parts of the pores (Fitts, 2002). At an interface between wetting and nonwetting fluid, the latter has the highest pressure and will therefore be the fluid that bulges.

The interface between two immiscible phases takes a form at which the potential energy of the system has a minimum value. The pressure difference is caused by the difference in interfacial forces of the two phases. This is called the interfacial tension (σ). When the pressure difference becomes too large, the interfacial tension is not strong enough to keep the system in equilibrium and the boundary will start to move.

The capillary pressure is linearly dependent on the interfacial tension and is described by the Young-Laplace equation (Fetter, 1999):

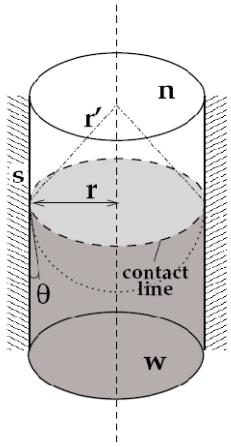

Figure 2.2 illustration of capillary pressure in a cylindrical tube

$$P_c = \frac{2\sigma}{r'}, \qquad (2.14)$$

where r' is radius of the mean curvature of the interface (see Figure 2.2).

When a cylindrical tube with radius r is considered, this equation becomes

$$P_c = \frac{2\sigma \cos \vartheta}{r} \qquad (2.15)$$

These equations hold at the microscale, but when considering the macroscale it becomes much more complex. A piece of soil does not consist of pores which all have the same shape and radius, but consists of all different kinds of pores. Since it is impossible to determine the shape and size of all pores, the microscale equations are not applicable at the macroscale.

At the macroscopic scale, the pressure of the wetting fluid for any block is defined as the volume-average pressure of this wetting fluid. Similarly, the pressure of the non-wetting fluid

is the average pressure of the non-wetting fluid within the volume. The macroscopic capillary pressure is then the difference between the average pressure of the non-wetting and of the wetting fluid:

$$P_c = P_n - P_w, \tag{2.16}$$

where P_c is the capillary pressure, P_n pressure of the nonwetting fluid and P_w is the pressure of the wetting fluid.

The macroscale capillary pressure is a function of saturation of the wetting phase. This is an empirical relationship that must be experimentally determined and is different for each soil type.

There are two well known models for the P_c-S relationship. One is the relationship found by Brooks and Corey (BC):

$$S_e = \frac{S_w - S_{wr}}{1 - S_{wr}} = \left(\frac{P_d}{P_c}\right)^{\lambda}, \quad \text{(Brooks and Corey, 1964)} \tag{2.17}$$

where S_e is the effective saturation, S_w is the saturation of the wetting phase, S_{wr} is the residual saturation of the wetting phase, P_d is the entry pressure, and λ is a BC parameter which is a measure of uniformity of the material and is empirically derived.

The second relationship was defined by Van Genuchten (VG) (1980):

$$S_e = \frac{S_w - S_{wr}}{1 - S_{wr}} = \left[1 + (\alpha P_c)^n\right]^{-m} \tag{2.18}$$

Where α and n are VG parameters, and m is defined as $1 - \frac{1}{n}$.

In Figure 2.3 the curves of both the BC and VG relationships are plotted. The main difference between the curves occurs at high saturations. According to the VG relationship, there is no capillary pressure for S =1. According to the BC relationship, capillary pressure has a value larger than 0 for S = 1. This value is defined as the entry pressure of a soil. Depending on the problem to be solved, a choice has to be made between the two relations.

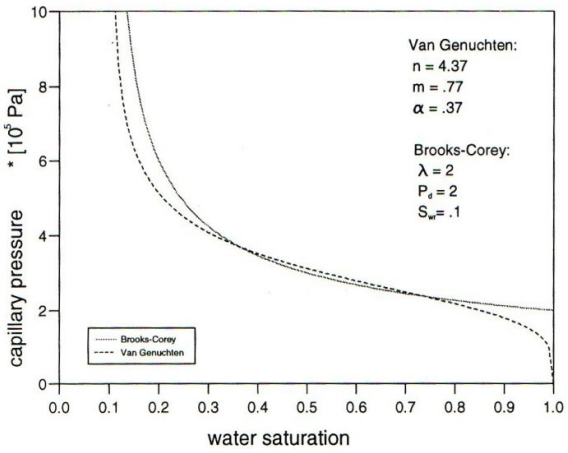

Figure 2.3 Pc(S)-relationship after Brooks-Corey and Van Genuchten, on equal physical conditions.

2.5 Relative permeability

When more than one fluid or gas is present in a porous medium, the flow of one component is influenced by the presence of the other components. The ability to flow of one component is called the relative permeability and is defined by the following relationship (Helmig, 1997):

$$k_{r\alpha} = \frac{k_\alpha}{\kappa}, \tag{2.19}$$

where $k_{r\alpha}$ is the relative permeability of phase α, k_α the absolute permeability of phase α and κ is the intrinsic permeability.

The relative permeability depends on the degree of saturation. When the saturation of a phase increases, more of the surrounding pores will be filled with that phase, such that the relative permeability increases. Since saturation is a function of capillary pressure, relative permeability can be defined as a function of capillary pressure as well. Quantitatively, this relationship is given by the following equations (Helmig, 1997):

For the wetting phase:

$$k_{rw}(S) = S^{A}\left[\frac{\int_{0}^{S}\frac{1}{\left[P_c(S^*)\right]^{B}}dS^*}{\int_{0}^{1}\frac{1}{\left[P_c(S^*)\right]^{B}}dS^*}\right]^{C} \tag{2.20}$$

For the nonwetting phase:

$$k_{rn}(S) = \left(1-S^{A}\right)\left[\frac{\int_{0}^{S}\frac{1}{\left[P_c(S^*)\right]^{B}}dS^*}{\int_{0}^{1}\frac{1}{\left[P_c(S^*)\right]^{B}}dS^*}\right]^{C} \tag{2.21}$$

There are two models that are generally used to describe the relative permeability-saturation relationship, one by Burdine (1953), and one by Mualem (1976). In the Burdine model A = B = 2, C = 1. In the Mualem model, A = 0.5, B = 1, C = 2.
Generally, the Brooks and Corey model is used in combination with the Burdine model, which yields:

$$k_{rw} = S^{\frac{2+3\lambda}{\lambda}} \tag{2.22}$$

$$k_{rn} = (1-S)^{2}\left(1-S^{\frac{2+\lambda}{\lambda}}\right) \tag{2.23}$$

The Van Genuchten model is generally used in combination with the Mualem model:

$$k_{rw} = S^{\varepsilon}\left[1-\left(1-S^{\frac{1}{m}}\right)^{m}\right]^{2} \tag{2.24}$$

$$k_{rn} = (1-S)^{\gamma}\left[1-S^{\frac{1}{m}}\right]^{2m} \tag{2.25}$$

The parameters ε and γ are form parameters which describe the connectivity of the pores. Typical values are $\varepsilon = \frac{1}{2}$ and $\gamma = \frac{1}{3}$ (Helmig, 1997).

In Figure 2.4 an example of relative permeability-saturation curves is depicted.

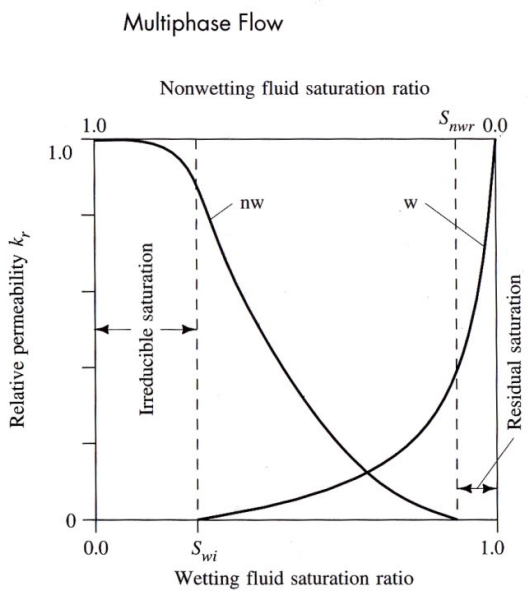

Figure 2.4. Typical relative permeability curves for a two-phase system.

3. Conceptual and mathematical model

The flow of natural gas in the unsaturated zone is a typical example of two-phase flow. Natural gas supplied in the Netherlands consists for 81.9% of CH_4 (methane), for 3.3% of higher hydrocarbons such as C_2H_6 (ethane), C_3H_8 (propane) and C_4C_{10} (butane), for 14% out of nitrogen and for 0.8% out of carbondioxide. To reduce complexity of the model, natural gas is assumed to consist of one single component: methane. As a result, the flow of gas in the unsaturated zone is a two phase flow problem, where the phases are water and gas and each phase can consist out of three components: water, air and methane.

3.1 Mass conservation equations

The mass conservation equation (2.10) which was given in Chapter 2 can be written for each component. In these equations the terms for diffusion and dispersion are also included.

Water component:

$$\begin{aligned}
&\phi \frac{\partial(\rho_{mol,w} X_w^w S_w + \rho_{mol,g} X_g^w S_g)}{\partial t} - \nabla \cdot \left\{ \rho_{mol,w} X_w^w \lambda_w \boldsymbol{\kappa_w} (\nabla \boldsymbol{P}_w - \rho_{mass,w} g_z) \right\} \\
&- \nabla \cdot \left\{ \rho_{mol,g} X_g^w \lambda_g \boldsymbol{\kappa_g} (\nabla \boldsymbol{P_g} - \rho_{mass,g} g_z) \right\} \\
&- \nabla \cdot (\phi S_g \boldsymbol{D}_{pm_g}^w \rho_{mol,g} \nabla X_g^w) - \nabla \cdot (\phi S_w \boldsymbol{D}_{pm_w}^w \rho_{mol,w} \nabla X_w^w) - q^w = 0
\end{aligned} \tag{3.1}$$

Air component:

$$\begin{aligned}
&\phi \frac{\partial(\rho_{mol,w} X_w^a S_w + \rho_{mol,g} X_g^a S_g)}{\partial t} - \nabla \cdot \left\{ \rho_{mol,w} X_w^a \lambda_w \boldsymbol{\kappa_w} (\nabla \boldsymbol{P}_w - \rho_{mass,w} g_z) \right\} \\
&- \nabla \cdot \left\{ \rho_{mol,g} X_g^a \lambda_g \boldsymbol{\kappa_g} (\nabla \boldsymbol{P_g} - \rho_{mass,g} g_z) \right\} \\
&- \nabla \cdot (\phi S_g \boldsymbol{D}_{pm_g}^a \rho_{mol,g} \nabla X_g^a) - \nabla \cdot (\phi S_w \boldsymbol{D}_{pm_w}^a \rho_{mol,w} \nabla X_w^a) - q^a = 0
\end{aligned} \tag{3.2}$$

Methane component:

$$\phi \frac{\partial(\rho_{mol,w} X^{m}_{w} S_w + \rho_{mol,g} X^{m}_{g} S_g)}{\partial t} - \nabla \cdot \left\{ \rho_{mol,w} X^{m}_{w} \lambda_w \boldsymbol{\kappa_w} (\nabla \boldsymbol{P}_w - \rho_{mass,w} g_z) \right\}$$
$$- \nabla \cdot \left\{ \rho_{mol,g} X^{m}_{g} \lambda_g \boldsymbol{\kappa_g} (\nabla \boldsymbol{P_g} - \rho_{mass,g} g_z) \right\}$$
$$- \nabla \cdot (\phi S_g \boldsymbol{D}^{m}_{pm_g} \rho_{mol,g} \nabla X^{m}_{g}) - \nabla \cdot (\phi S_w \boldsymbol{D}^{m}_{pm_w} \rho_{mol,w} \nabla X^{m}_{w}) - q^m = 0 \qquad (3.3)$$

,where $\rho_{mol,\alpha}$ is the molar density of phase α, X^c_α is the mole fraction of component c in phase α, and q^c is the concentration flux in $(kg/m^3)/s$ for each component c, which is the term for sources and sinks.

3.2 Thermal energy balance

The thermal energy balance equation describes the transport of heat in a system. Because all mass that is transported carries heat, there is a thermal energy term for every transport term. In addition to this, the porous medium can also conduct heat, which leads to an additional term.

$$\phi \frac{\partial(\rho_{mass,w} u_w S_w + \rho_{mass,g} u_g S_g}{\partial t} + (1-\phi) \frac{\partial \rho_s c_s T}{\partial t} - div(\lambda_{pm} grad T)$$
$$- div\left(\lambda_w \rho_{mass,w} h_w \boldsymbol{\kappa} (grad \boldsymbol{P}_w - \rho_{mass,w} g\right) - div\left(\lambda_g \rho_{mass,g} h_g \boldsymbol{\kappa} (grad \boldsymbol{P}_g - \rho_{mass,g} g\right)$$
$$- div(\boldsymbol{D}^{a}_{pm_g} \rho_{mol,g} h^{a}_{g} M^{a} grad\ X^{a}_{g}$$
$$+ \boldsymbol{D}^{w}_{pm_g} \rho_{mol,g} h^{w}_{g} M^{w} grad\ X^{w}_{g} + \boldsymbol{D}^{m}_{pm_g} \rho_{mol,g} h^{w}_{g} M^{w} grad\ X^{m}_{g}) - q^h = 0 \qquad (3.4)$$

where *u* is the specific internal energy, T is temperature, c_s is the average heat conductivity, h_α is the specific enthalpy, and M^c is the molecular mass of component c.

3.3 Mass transfer between phases

In the system that is described, two phases are present; a water phase and a gas phase. Each phase can comprise of three components, water, methane and air. As a result of evaporation and condensation of water or dissolution and degassing of air and methane there can be mass transfer between the two phases (Figure 3.1).

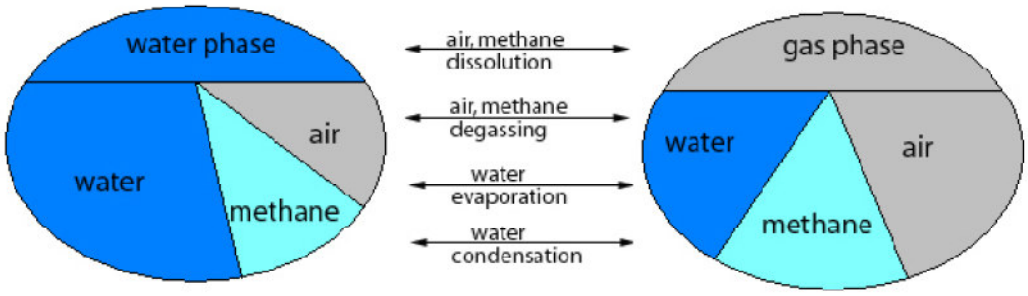

Figure 3.1 Diagram of mass transport between phases

There are some constitutive and closure relationships that are used to describe mass transfer between phases. One of these equations states that the sum of the water saturation and gas saturation must always be equal to one:

$$S_g + S_w = 1 \tag{3.5}$$

Another one states that the sum of all mole fractions in a phase must be equal to one:

water phase:

$$X_w^w + X_w^a + X_w^m = 1 \tag{3.6}$$

gas phase:

$$X_g^w + X_g^a + X_g^m = 1 \tag{3.7}$$

,

where X_α^c is the molar fraction of component c in phase α.

Similar to these equations is Dalton's law of partial pressures which states that the total pressure exerted by a gaseous mixture is equal to the sum of the partial pressures of each individual component in a gas mixture (Helmig, 1997). This law is empirically derived and is related to the ideal gas law:

$$P_g^w + P_g^a + P_g^m = P_g \tag{3.8}$$

The partial pressures can be calculated according to the ideal gas law:

$$P_g^\alpha = \frac{n_\alpha \cdot R \cdot T}{V} \tag{3.9}$$

,

where R is the universal gas constant, n_α is the number of moles, T is temperature, and V is volume.

To calculate the partial pressure of water in the gas phase, Raoult's law can be used as well, which states that the vapor pressure of an ideal solution is dependent on the vapor pressure of each chemical component and the mole fraction of the component present in the solution. The partial pressure of water in the gas phase can then be written as:

$$P_g^w = P_g \cdot X_g^w \tag{3.10}$$

Because a thermodynamic equilibrium is assumed it can be stated that the partial pressure of the water vapor corresponds to the saturation vapor pressure (Helmig, 1997);

$$P_g^w = P_{g,sat}^w \tag{3.11}$$

Equation (3.10) can then be rewritten as:

$$X_g^w = \frac{P_w^{sat}}{P_g} \tag{3.12}$$

If the concentration of a component is very small, such as the mole fractions of components air and methane in the water phase, Raoult's law is no longer valid. To calculate the partial pressures of air in the water phase Henry's law is used, which is valid for low concentrations (Helmig, 1997):

$$X_w^a = P_g^a \cdot H_w^a \quad , \tag{3.13}$$

where H is Henry's coefficient which is dependent on temperature and pressure and can be determined using:

$$H_w^a = (0.8942 + 1.47 \cdot e^{-0.04394 \cdot T}) \cdot 10^{-10} \quad \text{(Helmig, 1997),} \tag{3.14}$$

where T is temperature in ˚C.

Since there is no expression available for the calculation of Henry's coefficient for methane in water, the mole fraction of methane in water is calculated using the solubility function of methane in water, which is a function of total gas pressure (P_g), mole fraction (X_g^m) and temperature.

$$X_w^m = S_w^m(P_g, T, X_g^m) \tag{3.15}$$

Further explanation can be found in work of Dogan (2004).

As a result of this mass transfer between phases, density will vary with varying molar fractions as following:

$$\rho_{mass,g} = \rho_{mol,g}(X_g^a M^a + X_g^m M^m + X_g^w M^w) \quad (3.16)$$

$$\rho_{mass,w} = \rho_{mol,w}(X_w^a M^a + X_w^m M^m + X_w^w M^w) \quad , \quad (3.17)$$

where M^c is the molecular mass of component c.

3.4 Mathematical model

The mathematical model transfers the conceptual model to a mathematical formulation, which include the balance equation for mass conservation and energy as well as he system dependent equations of state. The model is based on four governing equations which are the three mass balance equations for the components water, air and methane (Equations 3.1, 3.2 and 3.3) and the thermal energy balance equation (Equation 3.4).

These governing equations give a total of eleven unknowns (X_w^w, X_w^a, X_w^m, X_g^w, X_g^a, X_g^m, S_g, S_w, P_g, P_w, T). To solve a system of eleven unknowns, eleven equations are needed. There are four governing equations. By rewriting and substituting the seven closure and constitutive relationships given in Chapters 2 and 3, and substituting them into the four governing equations reduces the number of eleven unknowns to four primary variables: P_g, X_g^m, T and S_w.

The closure relationships are:

Equation (2.16): $P_c = P_n - P_w$

Equation (3.5): $S_g + S_w = 1$

Equation (3.6): $X_g^w + X_g^a + X_g^m = 1$

Equation (3.7): $X_w^w + X_w^a + X_w^m = 1$

The constitutive relationships are:

Equation (3.10): $P_g^w = P_g \cdot X_g^w$

Equation (3.13): $X_w^a = P_g^a \cdot H_w^a$

Equation (3.15): $X_w^m = S_w^m(P_g, T, X_g^m)$

However, some of the original eleven unknowns will disappear depending on the available phase state. It is possible that there will be a switch from a two-phase three-component model to a one-phase three-component model. When water and gas exist at the same time, the system needs to be solved for the orginal 11 unknowns. When there is only a water phase there will be a primary variable switch for saturation of water (S_w) which will turn into mole fraction of air in the water phase (X_w^a) and the mole fraction of methane in the gas phase (X_g^m) will be replaced by (X_w^m). When there is only a gas phase there will be a primary variable switch such that the saturation of water (S_w) will change into the mole fraction of air in the gasphase (X_g^a).

For these primary variables boundary and initial conditions will be given such that the system can be solved numerically.

4. Numerical model

A system of highly non-linear partial differential equations can only be solved analytically for very simple cases. The resulting system of equations for the two-phase flow of gas given in Chapter 3 must therefore be approximated using numerical methods. The evolving algebraic equations can then be solved using efficient and fast solvers.

4.1 MUFTE-UG

For the numerical simulation of the problem the simulator MUFTE-UG (Helmig et al., 1998) was used. MUFTE-UG is a combination of MUFTE and UG which stands for **MU**ltiphase **F**low **T**ransport and **E**nergy model on **U**nstructured **G**rid. It is a numerical simulator which can be used for the simulation of isothermal and nonisothermal multiphase, multicomponent flow and transport in porous and highly heterogeneous or fractured media. It was developed by the Institute of Hydraulic Engineering (IWS) together with the Department of Hydromechanics and Modeling of Hydrosystems, University of Stuttgart, and the Technical Simulation group of Interdisciplinary Center for Scientific Computing (IWR), University of Heidelberg.
It is conceptually designed as a research code with a strictly modular and hierarchical architecture that allows the combination of different physical and mathematical concepts with a number of discretization and numerical methods (Figure 4.1). The MUFTE toolbox mainly contains the physical model concepts and discretization methods in porous and fractured porous media. UG provides data structures and fast solvers for the discretization of partial differential equations based on parallel, adaptive multigrid methods.

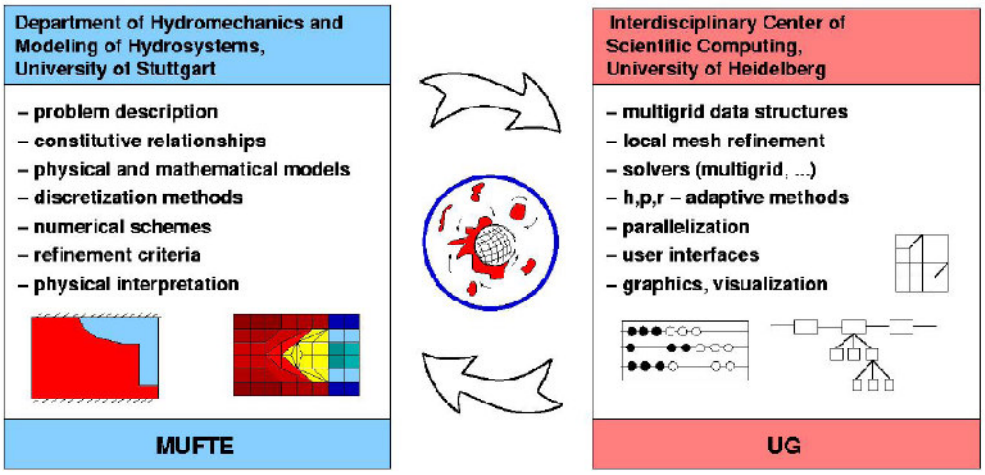

Figure 4.1 Concept diagrams of MUFTE and UG. Taken from Assteerawatt et al., 2005.

4.2 Discretization methods

Discretization concerns the process of transferring continuous models and equations into discrete counterparts. This process is carried out to make the model suitable for numerical evaluation. Discretization techniques in UG include a fully upwind box method in space. This box method will be further explained below. This explanation is taken directly from Manthey (2006).

In Section 2.2.3 the basic equations for the conservation of mass for multiphase flow are given. These continuous equations need to be discretized in space and time in order to solve them.

4.2.1 Discretization in space

The first step is to express the basic equation of mass conservation for multiphase flow in integral form over the domain Ω, which can be chosen freely:

$$\int_{\Omega} \phi \frac{\partial}{\partial t}(S_\alpha \rho_\alpha) dV = \int_{\Omega} \nabla \cdot \left[\rho_\alpha \lambda_\alpha \kappa \nabla (P_\alpha - \rho_\alpha g_z)\right] dV + \int_{\Omega} \rho_\alpha q_\alpha dV \qquad (4.1)$$

Where ρ_α is the density of phase α, which is assumed to be constant in both space and time.

The domain in which the mass balance equation should be solved is discretized in a number of domains by forming a primary mesh, which can also be denoted as Finite Element (FE). This primary mesh is an unstructured mesh which consists of a number of elements *m* all possessing a number of vertices *i*. Then a secondary mesh, called Finite Volume (FV) is generated for the formation of a control volume b_i around each vertex i. This control volume is formed by connecting an element's centre of gravity to the midpoint of the element edges and is called a BOX (Figure 4.2). The intersection of an element with a BOX is denoted sub-control volume. The spatial discretization method introduced here is called the BOX method.

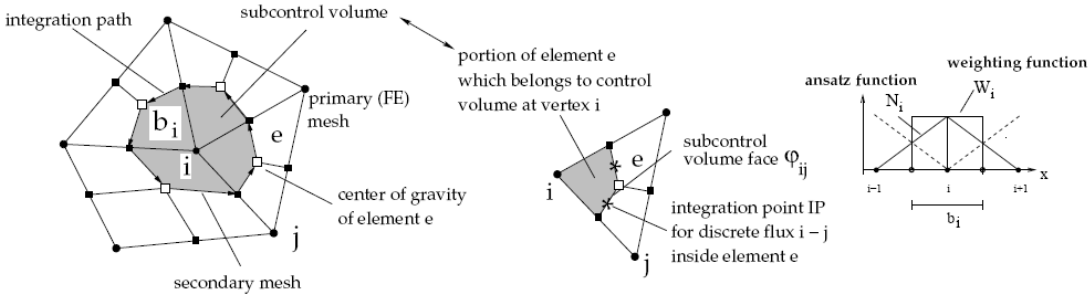

Figure 4.2 Primary (FE) mesh and construction of the secondary mesh as well as the basis and ansatz functions. Taken from Manthey (2006)

By introducing this numerical scheme the primary variables in the equation of mass conservation must be approximated by so called ansatz functions N_j. Within the BOX scheme

these are common Lagrangian polynomials, which are piecewise linear and continuous, but not continuously differentiable. The gas pressure P_g for example then can be approximated:

$$P_g \approx \sum_j P_{g\,j} N_j \tag{4.2}$$

where the gas pressure inside the sub-control volume is approximated by the sum of the gas pressures of the neighboring vertices *j* multiplied by the ansatz function N_j.

The gradient of the gas pressure can then be approximated by

$$\nabla P_g \approx \sum_{j\in\eta_j} (P_{g\,j} - P_{gi}) \nabla N_j \tag{4.3}$$

Where η_j is the set of neighboring vertices of vertex i.
The ansatz function which is visualized above in Figure 4.2 can be described as:

$$N_j(x_k) = \begin{cases} 1 & for \quad j = k \\ 0 & for \quad j \neq k \end{cases} \tag{4.4}$$

As a result the primary variables given in equation (4.1) are no longer a function of space.

Because of the approximation of the primary variables the balance equations can no longer be solved exactly anymore; the terms on the left-hand side of equation (4.1) are no longer equal to zero, but equal to a residual ε. This residual ε should be weighed in such a way that it becomes zero over the average domain. To do this, position-dependent weighing functions $W_i(x)$ are introduced. If one considers the principle of orthogonality, these should be chosen such that:

$$\int_\Omega W_i \varepsilon \, dV = 0 \quad for \quad i = 1,2,...,n_{nodes} \tag{4.5}$$

where W_i is the weighing function, which is visualized in Figure 4.2. For the BOX scheme the weighing functions are defined as piecewise constant so that

$$W_i(x) = \begin{cases} 1, & if \quad x \in b_i \\ 0, & if \quad x \notin b_i \end{cases} \tag{4.6}$$

Here b_i is the control volume around vertex i.

Now equation (4.1) can be rewritten as following:

$$\int_\Omega W_i \phi \sum_{j\in\eta_i} (S_\alpha \rho_\alpha)_j N_j \, d\Omega - \int_\Omega W_i \nabla \cdot \left[\rho_\alpha \lambda_\alpha \kappa \left\{ \sum_{j\in\eta_i} (P_{\alpha j} - P_{\alpha i}) - \rho_{\alpha ij} g \sum_{j\in\eta_i} (z_j - z_i) \right\} \nabla N_j \right] d\Omega$$
$$- \int_\Omega W_i \rho_\alpha q_\alpha d\Omega = 0 \tag{4.7}$$

Where z_i is the z-coordinate of vertex i.
By applying the midpoint-rule the first and the third term, which are the accumulation term and the source and sink term respectively, can be approximated:

$$\int_{\Omega} W_i \phi \sum_{j \in \eta_i} (S_\alpha \rho_\alpha)_j N_j d\Omega = \phi (S_\alpha \rho_\alpha)_i |b_i| \tag{4.8}$$

$$\int_{\Omega} W_i \rho_\alpha q_\alpha d\Omega = (\rho_\alpha q_\alpha)_i |b_i| \tag{4.9}$$

Where $|b_i|$ is the volume of control volume b_i.

The second term in equation (4.7) is the flux term. This term can be summarized to;

$$\int_{\Omega} W_i \nabla \cdot \boldsymbol{F} d\Omega \tag{4.10}$$

Where the flux is represented as **F**. By applying the product rule of differentiation:

$$\int_{\Omega} \nabla \cdot (W_i \boldsymbol{F}) d\Omega = \int_{\Omega} \nabla W_i \boldsymbol{F} d\Omega + \int_{\Omega} W_i \nabla \cdot \boldsymbol{F} d\Omega \tag{4.11}$$

this can be written as:

$$\int_{\Omega} W_i \nabla \cdot \boldsymbol{F} d\Omega = \int_{\Omega} \nabla \cdot (W_i \boldsymbol{F}) d\Omega - \int_{\Omega} \nabla W_i \boldsymbol{F} d\Omega \tag{4.12}$$

The second term on the right-hand side becomes zero for the chosen weighing functions W_i. The volume integral can then be conveyed to a boundary integral by applying the Gauss's Divergence Theorem

$$\int_{\Omega} \nabla \cdot (W_i \boldsymbol{F}) dV = \oint_{\Gamma} W_i \boldsymbol{F} \cdot \boldsymbol{n} d\Gamma \tag{4.13}$$

Where n is the unit normal vector.
By introducing the total potential $\psi_{\alpha i}$:

$$\Psi_{\alpha i} = \left(\sum_{j \in \eta_i} P_{\alpha i} - \rho_{\alpha i} g \sum_{j \in \eta_i} z_i\right) \tag{4.14}$$

the second term of equation (4.7) can be rewritten as:

$$\int_{\Omega} W_i \nabla \cdot \left[\rho_\alpha \lambda_\alpha \kappa (\Psi_{\alpha j} - \Psi_{\alpha i}) \nabla N_j\right] d\Omega = \oint_{\partial b_i} W_i \rho_\alpha \lambda_\alpha \kappa \Psi_{\alpha ij} \nabla N_j \cdot \boldsymbol{n} \, d\Gamma_{bi} \tag{4.15}$$

The difference in total potential between vertices *i* and *j* can be written as:

$$\Psi_{\alpha ij} = (\sum_{j\in\eta_i}(P_{\alpha j} - P_{\alpha i}) - \rho_{\alpha i} g \sum_{j\in\eta_i}(z_j - z_i)) \tag{4.16}$$

The internal fluxes are evaluated at the mid-point of a subcontrol volume face φ at the integration point IP (Figure 4.2) and then weighted on that face. The integration over the flux term of one box can thus be approximated by:

$$\boldsymbol{F}_i := \sum_{l\in e_i} \sum_{j\in\eta_i} (\rho_\alpha \lambda_\alpha)_{ij} \Psi_{\alpha ij} \nabla N_j \cdot \boldsymbol{n} \varphi_{ij}^{e_l} \tag{4.17}$$

An upstream weighting technique is applied to specify how the density ρ_α times the mobility λ_α is to be treated. This stabilizes the solution and hinders the infiltration on non-wetting phase into a part of the domain with high-entry pressure for sufficiently refined grids. The upstream direction is defined by:

$$(\rho_\alpha \lambda_\alpha)_{ij}^{ups} = \begin{cases} (\rho_\alpha \lambda_\alpha)_i & if \quad (\Psi_{\alpha j} - \Psi_{\alpha i}) \geq 0 \\ (\rho_\alpha \lambda_\alpha)_j & if \quad (\Psi_{\alpha j} - \Psi_{\alpha i}) < 0 \end{cases} \tag{4.18}$$

Finally the spatially discretised form of equation (4.1) can be written by closing the system with equations (2.18) and (3.5) ($S_w+S_n=1$) and solving for the primary variables P_w and S_n.

$$\begin{aligned} g_{\alpha,i}(P_{w,i}; S_{n,i}) := (-1)\delta^{\alpha,w} \phi (S_\alpha \rho_\alpha)_i |b_i| \\ - \sum_{l\in e_i} \sum_{j\in\eta_i} (\rho_\alpha \lambda_\alpha)_{ij}^{ups} \kappa (\Psi_{\alpha j} - \Psi_{\alpha i}) \nabla N_j \cdot n \varphi_{ij}^{e_l} \\ - (\rho_\alpha q_\alpha)_i |b_i| - m_{\alpha i} \end{aligned} \tag{4.19}$$

with:

$$\Psi_{\alpha i} = P_{w,i} + \delta^{\alpha,n} P_{c,i} - \rho_{\alpha i} g_{zi} \tag{4.20}$$

In this equation the term $m_{\alpha i}$ quantifies the flux over the boundary in case $\partial b_i \cap \Gamma_{\alpha,N}$. $\delta^{\alpha,w}$ and $\delta^{\alpha,n}$ are Kronecker delta's. The flux over the sub-control volume face of $b_i \cap b_j$ from box b_i into box b_j equals the opposite flux from box b_i to $b_i \cap b_j$, which shows that the method conserves mass locally.

4.2.2 Discretization in time

The just described coupled, highly non-linear equations need to be discretised in time as well. In this work a finite difference method is used and temporal discretization is carried out using

a fully implicit Euler scheme. The unknowns on time n+1 depend on each other and can not be solved in one step unlike explicit methods. There is no limit to the time step size considering the stability of the solution (Hinkelmann, 2003). However the time step should not be chosen too big considering the accuracy of the solution.

$$\frac{\partial u}{\partial t} \approx \frac{u^{n+1} - u^n}{\Delta t} \qquad \text{with} \quad \Delta t = t^{n+1} - t^n \tag{4.21}$$

The balance equation then becomes;

$$\begin{aligned} g_{\alpha,i}(P_{w,i}; S_{n,i}) := (-1)\delta^{\alpha,w} \frac{\phi}{\Delta t}((S_\alpha \rho_\alpha)_i^{n+1} - (S_\alpha \rho_\alpha)_i^n |b_i| \\ \sum_{l \in e_i} \sum_{j \in \eta_i} (\rho_\alpha \lambda_\alpha)_{ij}^{ups,n+1} \kappa (\Psi_{\alpha j}^{n+1} - \Psi_{\alpha i}^{n+1}) \nabla N_j \boldsymbol{n} \varphi_{ij}^{e_l} \\ - (\rho_\alpha q_\alpha)_i^{n+1} |b_i| - (m_{\alpha i})^{n+1} \end{aligned} \tag{4.22}$$

It is shown that the implicit Euler scheme is unconditionally stable independent on time step size (Bastian & Helmig, 1999). The discretised set of governing non-linear equations is linearized using the Newton-Raphson method. As diffusion systems are non-linear the Newton method exhibits a tendency to overestimate the update. This leads to intermediate results which can lie outside the convergence region of the Newton scheme or cause numerical problems which prevent convergence completely. MUFTE-UG tries to minimize this diffusion by using a time step control. A damping factor is introduced to minimize the overestimation and facilitate global convergence. Based on the performance of the damped inexact Newton scheme the time step is adjusted automatically. To determine the damping factor a line search is performed. The number of line searches necessary to determine the damping factor influence the time stepping. If the damping factor can be calculated within the first line search, the time step is multiplied by a factor. If, on the other hand, the damping factor cannot be determined after a given number of line searches, the time step is reduced. In MUFTE-UG the size of the first, the maximum and the minimum time step can be defined. If convergence cannot be achieved for the smallest time step, a simulation is aborted.

5. Numerical simulations

In this Chapter, gas migration through the soil is analyzed by means of numerical simulations. The multiphase flow and transport model MUFTE-UG discussed in Chapter 4 is used in an attempt to simulate gas migration through the unsaturated zone.
As stated before in Chapter 3, natural gas which is distributed in the Netherlands consists out of multiple components. To reduce complexity and thus calculation time of the model, gas is assumed to consist only out of one component, methane. The most significant soil properties that are used in the model, such as the water retention curve and water and gas relative permeabilities were taken from actual measurements and can be seen in Tables 5.1, 5.2 and 5.3.
Simulations have been performed to visualize the difference in spreading width and volumetric flux as a result of different variables. Since it is expected that spreading width and volumetric flux are influenced by water level, soil type and the size of the leakage, the influence of a change in each of these parameters is simulated separately. This way, it is tried to get a better understanding of the expected differences in spreading width and volumetric flux. Since it is not possible to create a grid that can simulate a leak smaller than 1 cm, the influence of the size of the leakage is simulated using different values for constant fluxes of gas flowing into the domain.
Next to the influence of these three major phenomena, simulations with variations in other parameters that are expected to be of influence, such as pressure in the pipeline and a variation in permeability of the soil, have been performed. It was also attempted to visualize the influence of precipitation, but this did not produce any reliable results.
Because the numerical model is very complex, parallel computation is necessary. This is done at SARA, the most advanced computer and network centre in the Netherlands.

5.1 Domain description

For the simulations, two different mesh types are used. The first mesh is a triangular one, called ART (Almost Regular Triangles). The second mesh used is a rectangular mesh, named RECTMESH. Differences and applications of these two mesh types are discussed below.
At the boundaries of the domain, boundary conditions must be given for the four primary variables gas pressure (P_g), mole fraction of methane in the gas phase (X_g^m) temperature (T) and water saturation (S_w). Two different types of boundary conditions can be given for all primary variables:

- a Dirichlet boundary condition, which gives the value of a variable at the boundary
- a Neumann boundary condition, which gives the value of the derivative of a variable at the boundary

5.1.1 Triangular mesh

ART mesh is a mesh build up of triangles with angles of approximately 60˚. The advantage of this mesh is that it is possible to make a local refinement. Due to the possibility to create a local refinement at the place of interest, it is possible to use a large domain for the calculations. This reduces the influence of any boundary effects.

The domain used for the simulations with ART mesh has a size of 10x10 meter. The bottom 80 cm of the domain is the area of interest in which the physical parameters vary with every simulation. The upper part of the domain has a much higher permeability and no diffusion in order to simulate open-air conditions. The domain with given boundary conditions and permeability values is shown in Figure 5.1.

The boundary condition at the source introduces a flow of gas, which consists mainly out of methane, into the domain as a result of a realistic pressure difference of 100 mbar.

5.1.2 Rectangular mesh

A rectangular mesh is used to produce a random permeability field and to create a continuous horizontal layer with a different permeability. Since it is not possible to apply a local refinement with this mesh, the domains used for simulations are smaller than the domain used with ART mesh. For the simulations with a low permeability layer, a domain of 2x2 m is used, for simulations with a random permeability field a domain of 5x1 m is used. A larger domain is not possible, since this would result in too large a computation time. The size of a grid cell is 2.5x2.5 cm in the 2x2 m domain, and 4x4 cm in the 5x1 m domain. As a result, the size of the leakage used in this simulations is larger than the leakage simulated with a triangular mesh.

The boundary conditions and permeabilities are the same as for the triangular mesh, and can be found in Figure 5.1.

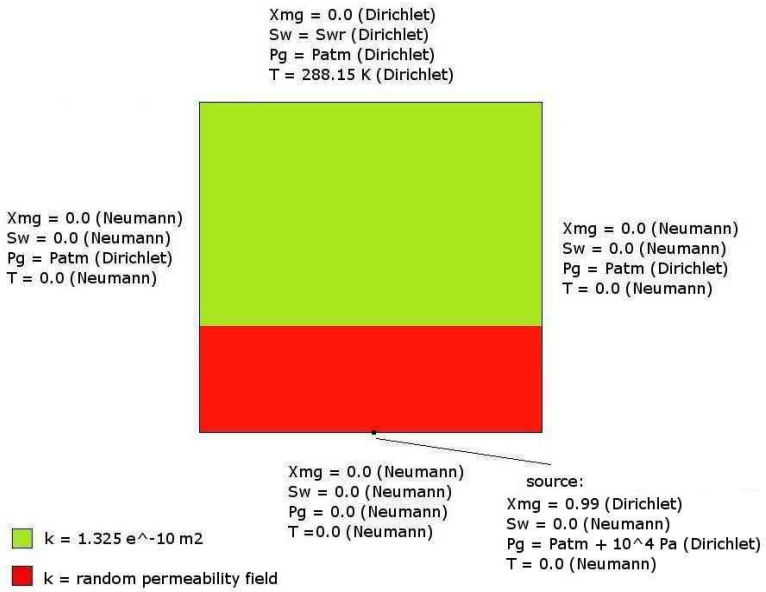

Figure 5.1 Domain with given permeabilities and boundary conditions

5. 2 Parameters for typical Dutch soils

In the numerical simulations, values of parameters for describing the physical properties of soils have to be given. In this study, the properties given by the Staringreeks are used (Wörsten et al. 2001). The Staringreeks is created by Alterra, a research institute which is part of Wageningen University and Research Centre. It gives characteristic values of water retention curves and permeabilities for Dutch top soils (Table 5.1) and is obtained by actual measurements form typical Dutch soils. The data are intended to be used for modeling studies and simulations (Wörsten et al., 2001).
As an average of these two soils in some simulations the properties from Bohne et al. (1992) are used (Table 5.2).

Texture class	**d_{50} (µm)**	**s_r (cm^3/cm^3)**	**φ (cm^3/cm^3)**	**α (1/cm)**	**n (-)**
Fine to medium fine sand	105-210	0.02	0.43	0.0234	1.801
Coarse sand	210-2000	0.01	0.36	0.0453	1.933

Table 5.1 Optimized values of parameters for describing average soil physical properties for sandy soils. Taken from the Staringreeks by Wörtsen et al., 2001.

Texture class	**d_{50} (µm)**	**s_r (cm^3/cm^3)**	**φ (cm^3/cm^3)**	**α (1/cm)**	**n (-)**
Medium sand	210-500	0.034	0.373	0.0363	3.03

Table 5.2 Optimized values of parameters for describing average soil physical properties for a medium sand. Taken from the Bohne et al. (1992).

In this study the retention curve of methane and water is assumed to be identical to the retention curve of air and water. This seems to be a legitimate assumption since capillary pressure between water and gas phase is mainly determined by the fact that there are only few molecules present in the gas phase. The difference in interaction of methane and air then has little effect (private communication with Prof. dr. ir. H. Bruining of the Delft University of Technology).
The water retention curves for the parameters of Wörsten et al. (2001) and Bohne et al. (1992) are shown in Figures 5.2 and 5.3.

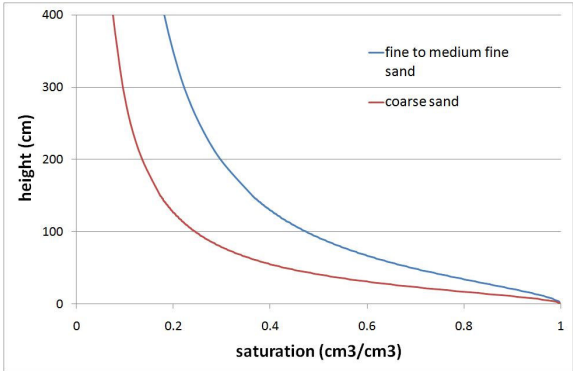

Figure 5.2 Water retention curve for fine and a fine and coarse sand (Staringreeks by Wörtsen et al. 2001)

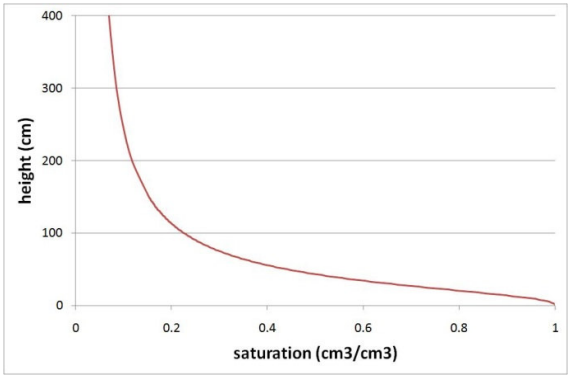

Figure 5.3 Water retention curve for medium sand (Bohne et al., 1992)

Another soil property that has to be given is intrinsic permeability. The values for intrinsic permeability for different grain sizes can be seen in Table 5.3 which is taken directly from Bear (1972).

$-\log_{10}$ · K(cm/s)	−2	−1	0	1	2	3	4	5	6	7	8	9	10	11
Permeability	Pervious				Semipervious				Impervious					
Aquifer	Good					Poor				None				
Soils	Clean gravel		Clean sand or sand and gravel			Very fine sand, silt, loess, loam, solonetz								
					Peat			Stratified clay		Unweathered clay				
Rocks					Oil rocks			Sandstone		Good limestone, dolomite		Breccia, granite		

$-\log_{10}$ · k(cm²)	3	4	5	6	7	8	9	10	11	12	13	14	15	16
$\log_{10} k$(md)	8	7	6	5	4	3	2	1	0	−1	−2	−3	−4	−5

Table 5.3 Typical values for hydraulic conductivity and intrinsic permeability. Table taken from Bear (1972).

5.3 Numerical simulations

5.3.1 Influence of soil heterogeneity on the migration of gas

When a wetting front advances through an unsaturated soil, soil heterogeneities can lead to distinct fingering phenomena (Conciani et al., 1995). In the case of gas leaking from a low pressure distribution pipe the process is not the same, since it is a non-wetting front that is forced through an initially saturated or unsaturated soil at a constant pressure of 100 mbar. Although the process is not the same, similar phenomena can be expected. In both cases it is

expected that high permeability paths within the soil control the advance of either a wetting or a non-wetting front.
To model the influence of soil heterogeneities on the flow of gas, simulations have been performed with a rectangular mesh. In one of these simulations a random permeability field was created by a program called SIMSET. With this program a random permeability field can be generated by giving the average permeability, variance and correlation length.
In this simulation the parameters for a fine sand are used (Staringreeks, Table 5.1). The values for intrinsic permeability are taken from Bear (1972) (Table 5.3).
Two simulations have been performed, with the water level at the same height as the leakage. In the first simulation a homogeneous soil is used, whereas in the second simulation a heterogeneous soil is used. The average permeability of this soil is the same as the permeability of the homogeneous soil ($1.0 \cdot 10^{-13}$ m^2). The minimum permeability of the soil is $4.35 \cdot 10^{-16}$ m^2, the maximum permeability is $3.0 \cdot 10^{-11}$ m^2. The random permeability field is depicted in Figure 5.4.

Simulations are conducted until steady state conditions are reached, which means that the flux flowing into the domain is equal to the flux flowing out of the domain.

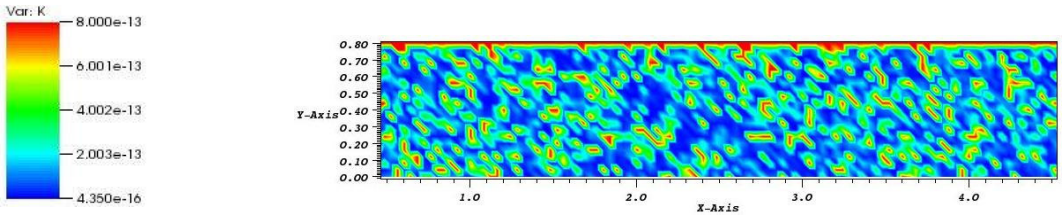

Figure 5.4 Random permeability field used for the simulation of a heterogeneous soil

5.3.1.1 Results

Figure 5.5 shows the distribution of methane in the homogeneous and heterogeneous soil after 18 minutes. The front of the methane in the homogeneous soil is smooth, whereas the front of the methane in the heterogeneous soil shows some irregularities, but no distinct fingers. At steady state conditions, after approximately 3 days (Figure 5.6), the spreading widths of the high concentration zone of methane is approximately 1.5 meter in both the homogeneous and the heterogeneous field. However the methane flux flowing out of the homogeneous domain is approximately 30% larger than the methane flux out of the heterogeneous domain

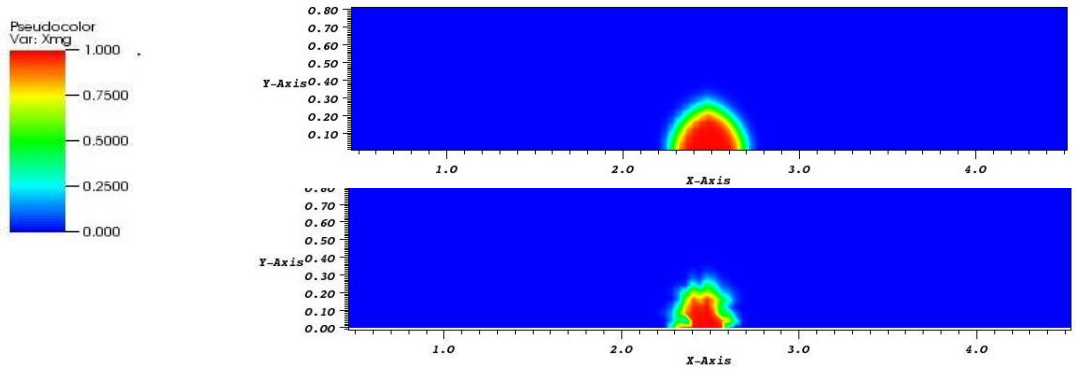

Figure 5.5 Mole fraction of methane in the gas phase after 18 minutes a) in a homogenous soil with an average permeability for a Dutch soil, b) as a result of a random permeability field with values for an average Dutch soil

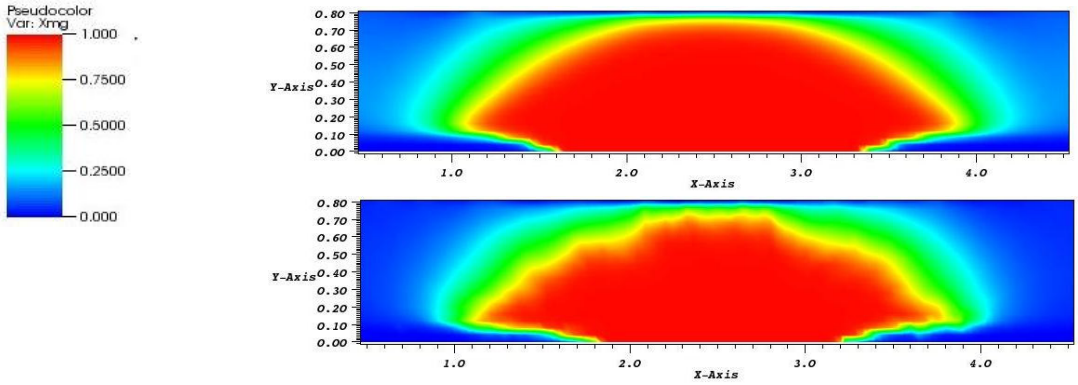

Figure 5.6 Mole fraction of methane in the gas phase at steady state as a result of a) a homogeneous permeability field with an average permeability for a Dutch soil, b) a random permeability field with values for an average Dutch soil

5.3.1.2 Discussion and conclusions

The results of the simulation with a heterogeneous soil are very similar to the results of the simulation with a homogeneous soil. Total spreading width of the gas is approximately equal in both simulations. This indicates that using a homogeneous permeability field does not result in a different spreading. The random permeability field only slightly influences the spreading of the gas by creating irregularities at the front of the spreading.

No distinct preferential flow paths are formed. This does not imply that no preferential flow paths will form in the field. In Chapter 6.3 experiments are discussed where the existence of preferential flow paths is shown. The lack of preferential flow paths in the simulation is probably due to the size of the grid cells. In this simulation grid cells of 4x4 cm are used. As a result, there can only be a difference in permeability every 4 cm. In reality, permeability is a

microscale phenomenon and will be different in every pore. To be able to model natural soil heterogeneities in a realistic way, smaller grid cells are necessary. Delahaye and Alonso (2002) used grid cells of 2x2 mm and showed that natural soil heterogeneities can cause for preferential flow paths to occur. Since it is currently not possible with MUFTE-UG to model the problem with such small grid cells due to capacity problems, it is decided that for the other simulations no random permeability field will be used.

The shape of the spreading of the gas is assumed to be a result of a variation in saturation in the domain. Because the water level is at the height of the leakage there is a typical distribution of water saturation in the domain as a result of capillary rise. As can be seen in Figure 5.2 the saturation of water will be much higher in the bottom of the domain. As a result relative permeability of the gas will be smaller in these bottom regions. This is expected to influences the spreading width of the gas. A more extensive discussion of the influences of saturation will be given in Section 5.3.4.

The total flux measured at the surface is about 30% higher for a homogenous soil than the flux resulting from a heterogeneous permeability field. It is unclear whether this is a result that is observed in the field as well, or if this is a simulation error. Since the fluxes are not used quantitatively in this research, but are only used to compare different fluxes qualitatively, the larger flux as a result of a homogeneous permeability field will not influence the results of the simulations.

5.3.2 Influence of pressure differences in the pipeline on the migration of gas

Although in most distribution pipes there is a pressure of 100 mbar, there are also distribution pipes with lower pressures. Pressures as low as 30 mbar can be present. To visualize the differences in spreading caused by a difference in pressure, two simulations are conducted. Both simulations are performed in the triangular mesh for a soil with parameters for a medium sand (Table 5.2) and a water level at the height of the leakage. In the first simulation a pressure of 100 mbar is applied at the leakage, in the second simulation a pressure of 30 mbar is applied. Simulations are run until steady state conditions are reached.

5.3.2.1 Results

As can be seen in Figure 5.7, a gas pressure of 100 mbar results in a larger spreading width at steady state conditions than a gas pressure of 30 mbar. In this situation a gas pressure of 30 mbar results in a maximum radial spreading of 2 meter from the leakage. A gas pressure of 100 mbar results in a maximum spreading of approximately 3.5 meter from the leakage.
The volumetric fluxes measured at the surface for steady state conditions are ten times higher for a gas pressure of 100 mbar then for a gas pressure of 30 mbar.
The time for steady state conditions to set in differs for different gas pressures. As a result of a larger gas pressure (100 mbar), flow velocities increase and steady state conditions are reached in approximately twelve hours. With a gas pressure of 30 mbar it takes approximately one day to reach steady state conditions.

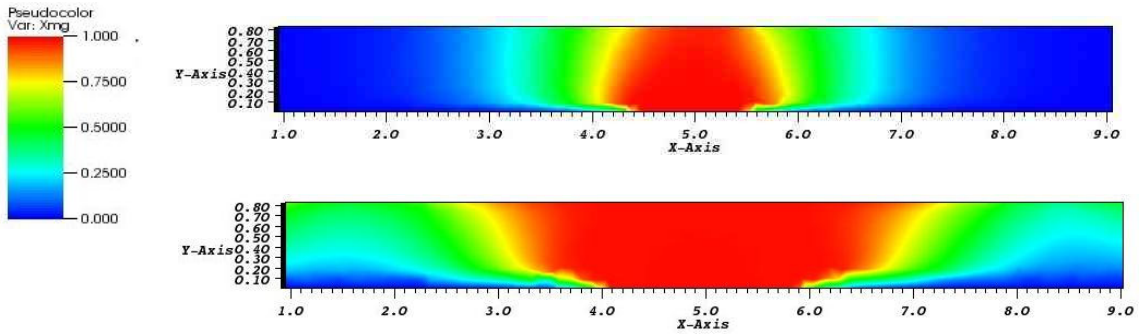

Figure 5.7 Mole fraction of methane in the gas phase at steady state as a result of different pressures in a pipeline: a) 30 mbar b) 100 mbar

Looking at the gas pressure distribution in the domain (Figure 5.8), it becomes clear that when a larger gas pressure is applied, a pressure gradient is present at a larger distance from the leakage. Because of the chosen scale, pressures larger than $1.010*10^5$ Pa are not visible in the figure.

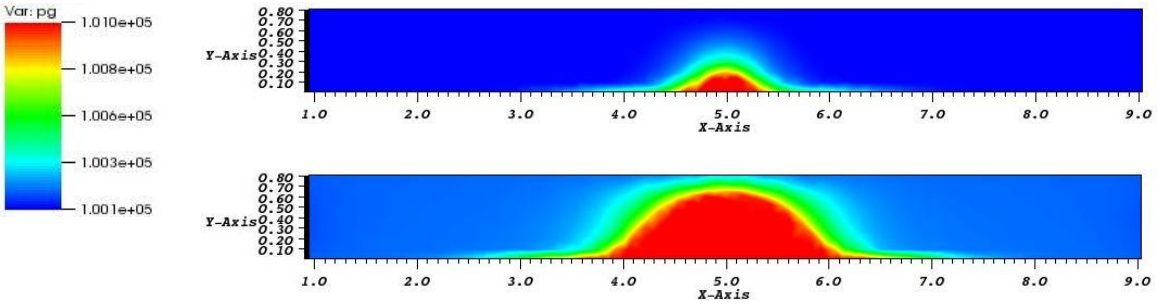

Figure 5.8 Gas pressure in Pascal at steady state as a result of different pressures in a pipeline: a) 30 mbar, b) 100 mbar

5.3.2.2 Discussion and conclusions

An increase in gas pressure in the pipeline results in a larger volumetric flux measured at the surface and a larger spreading width of the gas. Using MUFTE it is possible to quantify the volume flux of methane at the surface, but because only two-dimensional simulations are done, these do not give very realistic values. The values do however allow for comparison between different situations.

The wider spreading is the result of the pressure gradient, which at higher pressures is present at a larger distance from the leakage. Because an increase in gas pressure leads to an increase in total pressure gradient, an increase in gas pressure will also result in an increase in volumetric flux measured at the surface. This is also in accordance with the results obtained in the experiments. Because only two simulations are conducted no quantitative correlation

between gas pressure and spreading width can be determined. More simulations with varying pressure are recommended.

What has to be kept in mind is that it is not always possible for gas to enter the domain as a result of capillary and water pressure. This is dependent on grain size and water level and of course gas pressure in the pipeline. This will be discussed more extensively in Section 5.3.4.

5.3.3 Influence of the value of a constant flux on the migration of gas

Generally the size of a leakage is assumed to influence the spreading of gas through a soil. Since it is not possible to create a grid that can simulate a leak smaller than 1 cm, the influence of the size of the leak is simulated by using different values for constant fluxes of gas flowing into the domain. To determine the influence of flux value on the flow of gas through the soil, three simulations are performed using ART mesh. In the three simulations all conditions are equal (residual saturation, properties of medium sand from Table 5.2). The only difference is the value of the flux of natural gas flowing into the domain. Under equal conditions the value of the flux flowing into the domain is assumed to be related to the geometry of the leakage: the larger the size of the leakage, the larger the flux flowing into the domain.

The three different fluxes inserted are:

- 5 liter/hour
- 15 liter/hour
- 65 liter/hour

These are measured fluxes in the field and are therefore assumed to be realistic values. Simulations are conducted until steady state conditions are reached.

5.3.3.1 Results

At the start of the simulations a radial distribution of gas in the domain is observed. When the methane reaches the surface, the spreading rate of the gas in the horizontal direction decreases until steady state conditions are reached. With a flux of 65 liter/hour steady state conditions are reached after approximately two days, with a flux of 15 liter/hour steady state is reached after approximately three days. With a flux of 5 liter/hour steady state is reached after approximately five and a half days. These steady state conditions can be observed in Figure 5.9. Note that the total spreading width of the gas doesn't seem to change with increasing volume flux.

An increase in volume flux does result in a steeper concentration gradient (Figure 5.9). With a volumetric flux of 5 liter/hour a mole fraction of methane in the gasphase of 0.25 can be observed in a circle with a radius of 1.5 m measured from the leakage. The highest mole fraction observed at the surface is 0.5.

With a constant volumetric flux of 15 liter/hour a mole fraction of methane in the gasphase of 0.25 can be observed in a radius of 2.5 m from the leakage. Above the leakage the gasphase consists for approximately 85% out of methane.

With a volumetric flux of 65 liter/hour a mole fraction of methane in the gasphase of 0.25 can be observed in circle with a radius of approximately 3 m from the leakage. Above the location of the leakage the gas phase consists solely out of methane.

Looking at the gas pressure distribution in the domain (Figure 5.10), it becomes clear that when a larger flux is inserted, a steeper pressure gradient is present in the domain, although no large differences in maximum gas pressure are observed in the simulations. The maximum gas pressure observed at a volumetric flux of 65 liter/hour is $1.008 \cdot 10^5$ Pa. The maximum gas pressure observed at a volumetric flux of 15 liter/hour is $1.002 \cdot 10^5$ Pa and the maximum gas pressure observed at a volumetric flux of 5 liter/hour is $1.001 \cdot 10^5$ Pa. It is notable that the total width over which a pressure gradient is present is similar in all three simulations.

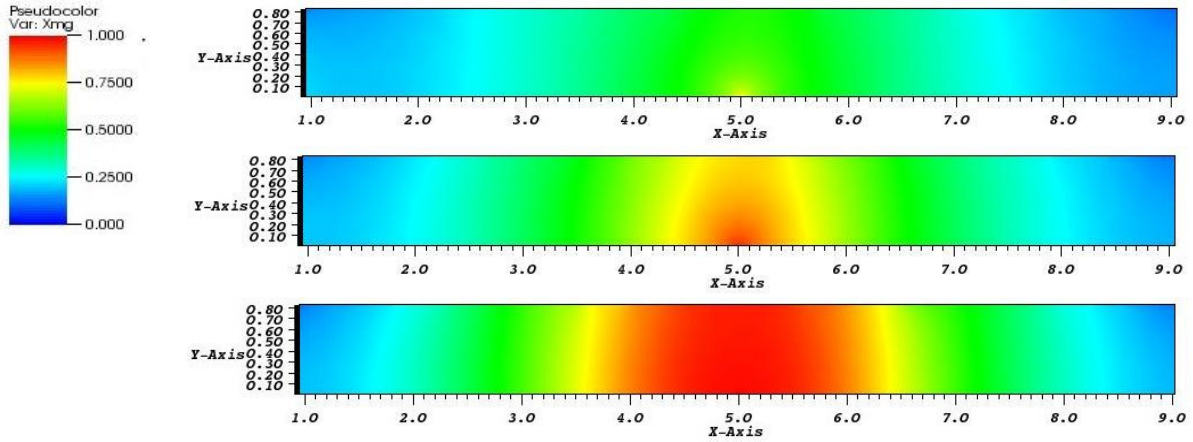

Figure 5.9 Mole fraction of methane in the gas phase at steady state as a result of different constant volume fluxes flowing into the domain: a) 5liter/hour, b) 15 liter/hour, c) 65 liter/hour.

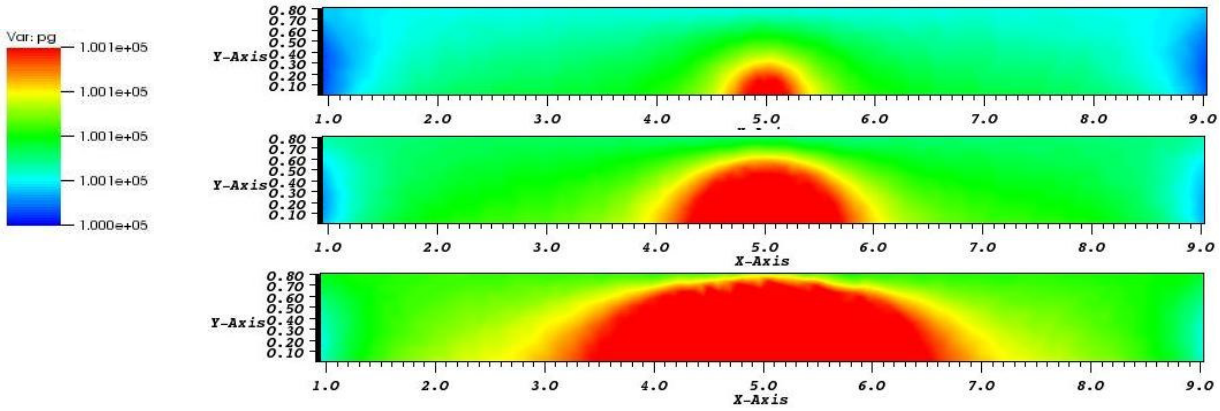

Figure 5.10 Gas pressure in Pascal at steady state as a result of different constant volume fluxes flowing into the domain: a) 5 liter/hour, b) 15 liter/hour, c) 65 liter/hour.

5.3.3.2 Discussion and conclusions

Because a steeper pressure gradient is present with increasing flux, the flow velocity of the gas will increase with increasing flux. As a result a steeper concentration gradient will be present in the domain. Because the total width over which a pressure gradient is present is approximately equal in all simulations, no change in total spreading width of the gas will occur.

As a result of a larger influx, flow rates of the gas increases as well. Steady state conditions are therefore reached in less time when the volume flux is larger. At steady state conditions the flux flowing out of the domain is equal to the flux flowing into the domain. Larger concentrations will thus always be observed at the surface when there is a larger flux.

Because under equal conditions the value of the flux flowing into the domain is assumed to be related to the geometry of the leakage and no increase in total spreading width is expected with increase in volume flux, no increase in spreading width is expected with increase in size of the leakage. However a steeper concentration gradient and a larger volumetric flux is expected.

5.3.4 Influence of degree of saturation on the migration of gas

Because relative permeability of the gas phase is dependent on the degree of saturation in the soil, saturation is expected to have a large influence on the flow of gas. To determine the influence of saturation on the flow of gas, three simulations for three different degrees of saturation have been performed using a triangular mesh. For the simulation the fine to medium fine sand parameters from Alterra (Table 5.1) are used. To be able to determine the influence of saturation between different grain sizes simulations for a coarse sand (Table 5.1) were attempted. Unfortunately, these simulations were not successful.

Because degree of saturation is dependent on water level, three different water levels have been used for these simulations:

- A water level at 20 cm above the bottom of the domain
- A water level at the bottom of the domain
- A deep water level which results in a residual saturation

5.3.4.1 Results

In Figure 5.11 the steady state situations for the three different degrees in saturation can be observed. As can be seen in Figure 5.11, a higher water level results in a decrease in spreading width of the gas.

The total spreading in a soil with a residual saturation at steady state is approximately 3 meters from the leakage. The maximum spreading width of the natural gas when the water level is at the bottom of the domain is approximately 2.3 meters and the maximum spreading width of the gas when the water level is 20 cm above the inlet is approximately 1.8 meters from the leakage. Notable is that the spreading width of the high concentration zone is approximately 1 meter for all simulations.

When looking at Figure 5.11, a difference in shape of the spreading is visible for the three different situations. A residual saturation results in an almost horizontal concentration gradient. With an increase in water level the width of the spreading seems to increase with

height, although a small decrease in spreading width is again observed at the top of the domain.

Only when there is a residual saturation, a steady state situation seems to be reached. For the other two situations there is a point where the gas flowing out of the domain is equal to gas flowing into the domain. However, the fluxes in and out of the domain keep increasing. Since these increasing fluxes do not result in a significant wider spreading, steady state is assumed when the influx equals the flux flowing out of the domain.
When there is a residual saturation steady state conditions are reached within one day. When the water level is at the bottom of the domain steady state conditions are reached after approximately three days. When the water level is 20 cm above the bottom of the domain steady state is reached after approximately five days.
Volumetric fluxes of natural gas observed at the surface of the domain at steady state conditions increase with decreasing degree in saturation With a residual saturation the volumetric gas flux is two times larger than when the water level is at the bottom of the domain and three times larger than at a water level of 20 cm above the gas inlet.

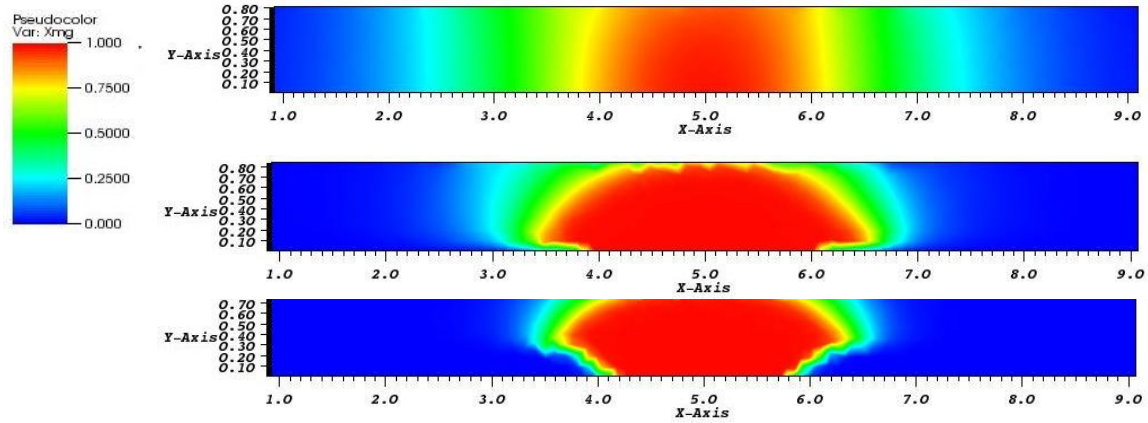

Figure 5.11 Mole fraction of methane in the gas phase at steady state as a result of differences in degree of saturation in the domain: a) residual water content, b) water level at the bottom of the domain, c) water is level is 20 cm above the bottom of the domain

5.3.4.2 Discussion and conclusions
From these simulations it can be concluded that an increase in saturation leads to a decrease in total spreading width of the gas.
An increase in saturation leads to a decrease of relative permeability of the gas. For gas it is easier to flow through zones of higher relative permeability. Flow velocities will increase as a result of an increase in relative permeability. As a result there will be a wider horizontal spreading of the gas at low saturations. This explains the shape of the spreading which increases with decreasing saturation. The fact that the width of the spreading seems to decrease at the top of the domain could be a result of higher flow velocities at that point.

Because gas can flow out more easily than it can enter that part of the domain, the concentrations of methane in the gas phase will be smaller in the top of the domain.
Due to increased flow velocities as a results of increased relative permeability of the gas steady state conditions will be reached in a shorter time span when the saturation decreases.

It can also be concluded that a higher water table results in a lower volumetric flux of methane measured at the surface of the domain. This is also due to the decreased relative permeability of the gas. The fact that no steady state conditions are reached in the situations where the degree of saturation is higher than residual is due to the fact that water dissolves in the methane. This results in a continuous decrease in saturation and a continuous increase in volumetric flux of gas entering the domain. This however is a very slow process and does not lead to a significant larger spreading width.

When Figure 5.11 b. is compared to Figure 5.7 b. a differences in spreading shape is noted. In these simulations saturation conditions are equal, but a different grain size is simulated (Figure 5.7 shows a simulation for a medium sand, Figure 5.11 for a fine sand).
In Figure 5.7 no decrease, but an increase in spreading width is observed at the top of the domain. This is probably a result of the difference in water retention curve for the different soil. For medium sand the degree in saturation is much lower in the top of the domain than for fine sand (Figures 5.2 and 5.3). This will result in a higher relative permeability for gas in the top of the domain, which results in a larger flow velocity and a wider spreading of the gas.

As stated before, the water table can reach a certain height, at which a gas pressure of 100 mbar will not be high enough to overcome the water pressure and capillary pressure and no flow will occur. However, in this model, it is not possible to insert water pressure as a result of a water layer, because this is a one phase phenomenon. Since a two-phase flow model is used, other physical laws apply. The transition from one set of physical laws to another set of physical laws is called multiphysics. MUFTE-UG is in its current state not capable to deal with multiphysics. As a result, water pressure is not taken into account and gas can always flow into the domain. However, the entry pressure of the soil is known and therefore the water height at which methane will no longer flow out of the leakage can be calculated. Only simulations with a water table at which methane is able to flow out are performed. As a result the volumetric flux at the surface will probably give a higher value than in the field, but this can be interpreted as a worst case scenario showing the maximum spreading width and flow velocities.

5.3.5 Flow of gas through an unsaturated soil with a low permeability layer on top of the surface

As a result of pavement, grass of frost op top of a soil a low permeability zone can occur on top of a soil. Because such a low permeability zone is expected to influence the flow of gas through the soil, a number of simulations have been performed to investigate the influence of such a zone.
All simulations have been performed using a rectangular mesh, which allows a continuous horizontal layer to be formed on top of the soil. Parameters for a medium sand (Table 5.1), an

intrinsic permeability of $1.3 \cdot 10^{-13}$ m^2 and a residual water saturation are used. The flow of gas is a result of a 100 mbar gas pressure difference.
Several top layers have been simulated:

- a layer with an intrinsic permeability of $6.3 \cdot 10^{-14}$ m^2
- a layer with an intrinsic permeability of $6.3 \cdot 10^{-15}$ m^2
- a layer with an intrinsic permeability of $1.3 \cdot 10^{-15}$ m^2
- an impermeable layer with an intrinsic permeability of 0 m^2

In the simulation with a layer of zero permeability, there is a hole created in this layer between x = 3.2 m and x = 3.5 m. Along this line, permeability is the same as the permeability in the domain below.

5.3.5.1 Results

When the top layer has a permeability of $6.3 \cdot 10^{-14}$ m^2, the low permeability layer does not seem to have much influence on the spreading of the gas. The gas can flow through the low permeability layer and only a small amount of gas accumulates under the low permeability layer (Figure 5.12 a).
When the intrinsic permeability of the low permeability layer is decreased to $6.3 \cdot 10^{-15}$ m^2, gas accumulates under the low permeability layer and the spreading width of the gas under the layer increases (Figure 5.12 b). Gas can however still flow through the low permeability layer.
When the intrinsic permeability of the low permeability layer is decreased further to form a low permeability layer with an intrinsic permeability of $1.3*10^{-15}$ m^2 the spreading width of the gas beneath the low permeable layer increases. Gas will eventually flow through the layer, but the gas is no longer coming from one point, but seems to flow out through the entire layer (Figure 5,12 c).
As can be seen in Figure 5.12 d, methane accumulates under the layer with zero permeability and spreads horizontally under the impermeable layer until it can escape through a high permeable zone.

Unfortunately in these simulations no steady state conditions could be reached, because of the limited size of the domain.

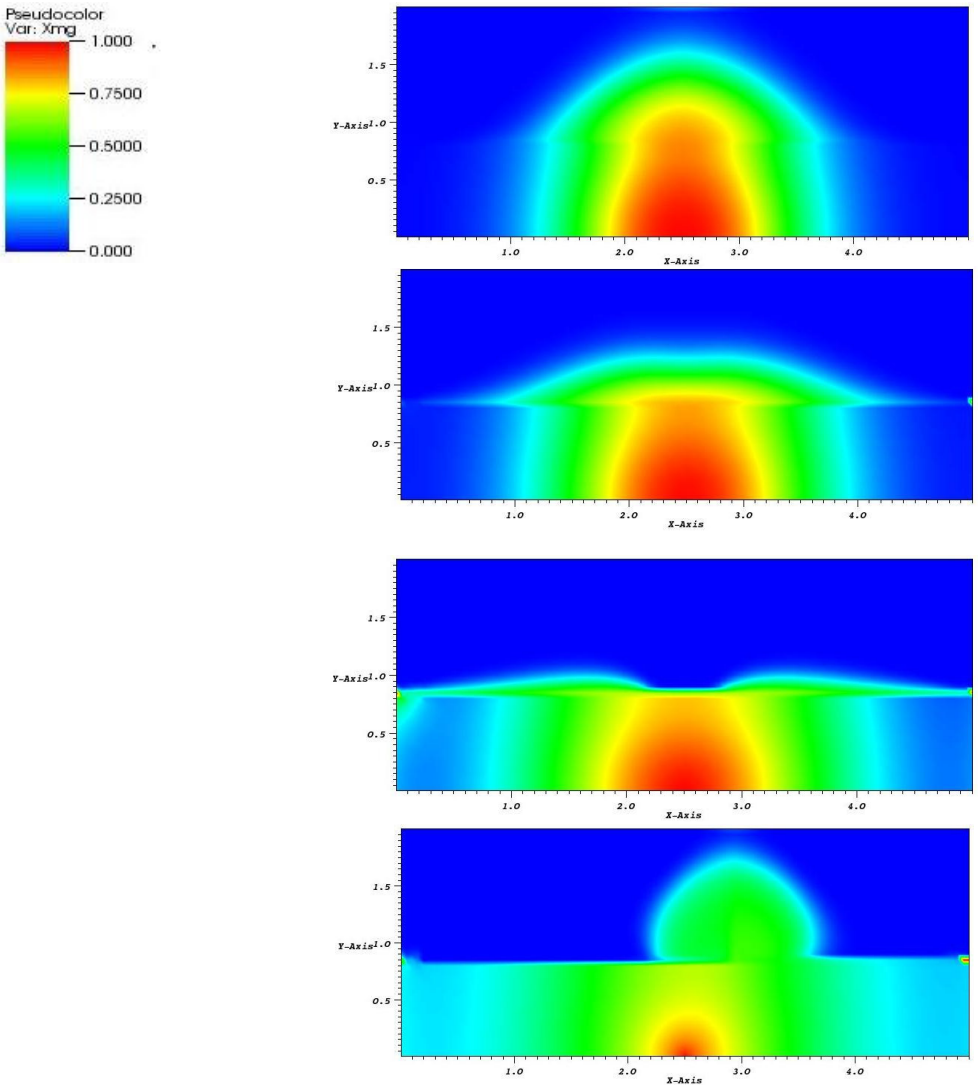

Figure 5.12 Mole fraction of methane in the gas phase with different low permeability layers on top of the soil (at 80 cm): a)intrinsic permeability of the layer is $6.3 \cdot 10^{-14}$ m^2 , b)intrinsic permeability of the layer is $6.3 \cdot 10^{-15}$ m^2 , c) intrinsic permeability of the layer is $1.3 \cdot 10^{-15}$ m^2, d) intrinsic permeability of the layer is zero, with a hole between x=3.2 and x=3.5.

5.3.5.2 Discussion and conclusions

The results indicate that the existence of a low permeability layer on top of a soil can result in an increase of total spreading width of the gas.

Simulations show that a significant increase in spreading width is obtained when the intrinsic permeability of this layer is at least 500 times smaller than the permeability in the domain. This corresponds to the difference between a fine and coarse sand.

When the permeability of the top layer is 1000 times smaller than the permeability of the soil gas can still flow through the top layer, but it no longer seems to appear from a point source. Determining the location of the leakage will then be more difficult.

An impermeable layer will cause horizontal spreading of the gas until a high permeability zone appears on top of the soil. Gas will thus only flow out of the domain when there is an interruption in the low permeability layer or when the layer ends.

Since the domain for the simulation was only 5 m wide, no quantitative results on the total spreading width for different layers can be given. However, under an impermeable layer it is expected that gas will continue to spread horizontally and only flow upward if an interruption in the low permeability layer occurs.

5.3.6 The influence of grain size on the migration of gas

An attempt was made to model the flow of gas through the two soil types from the Staringreeks (Table 5.1). However, it turned out that the program in its current state is not capable to deal with the large permeabilities typical for coarse sands. To say something about the influence of grain size on the flow of gas, a simulation with a very low permeability ($1.3 \cdot 10^{-16}$ m^2) has been performed. This permeability is typical for a clay. A residual saturation was used for this simulation.

5.3.6.1 Results

The simulation with the low permeability did not reach steady state conditions. The simulation stopped when 80% of the methane flowing into the domain was flowing out of the domain. This is after 28 days. Comparing this result with the result obtained from the simulation with the fine sand from the Staringreeks (Figure 5.13), it is clear that the width of spreading increases with increasing grain size.

The total spreading width of the gas in a fine sand when 80% of the methane flowing into the domain is flowing out of the domain is approximately 1.5 meter from the leakage. For clay this is approximately 1 meter.

The amount of methane flowing out of the domain is 18 times larger for the fine sand than for clay.

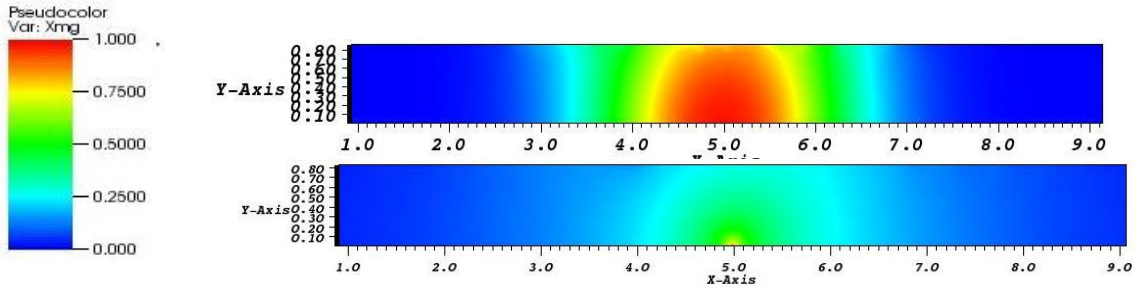

Figure 5.13 Mole fraction of methane in the gas phase for different grain sizes when the flux flowing out of the domain is 80% of the flux flowing into the domain for: a) fine sand, b)clay

5.3.6.2 Discussion and conclusions

From this simulation it is clear that a larger grain size results in a larger spreading with and a larger flux. An increase in spreading width with increasing grain size is also observed when comparing Figures 5.7 b. and 5.11 b. are compared. How wide the spreading will be at steady state conditions is not clear. It is probably a bit wider than in Figure 5.13b, and will be approximately 1.5 meters. This is considerably smaller than the spreading width of 3 meters for the fine sand from the Staringreeks. This indicates that when a coarse sand is used, spreading width will be considerably larger than for a fine sand.

5.3.7 Influence of precipitation on the migration of gas

It is also attempted to visualize the effect of precipitation on the migration of gas. However, all the attempts to simulate precipitation have not been successful. In its current state, MUFTE-UG seems incapable to deal with a sudden large increase in water saturation. In Chapter 7, experiments performed by Brötzenberger et al (1987) on the effect of rain on the spreading of methane are discussed.

6. Experiments

In Chapter 5 numerical simulations of the flow of gas through the unsaturated soil are described. In addition to these numerical simulations three small-scale experiments are conducted, which is described in this Chapter. The goal of these experiments is to obtain more insight on the mechanisms that are important for the flow of gas through the unsaturated zone. A comparison between the results of the experiments and outcomes of the numerical simulations is made.

6.1 One-dimensional column experiment

For flow of gas to occur through the soil, the gas pressure at the location of the leakage must be larger than the water pressure and capillary pressure combined at that point. Water pressure is the pressure on the bottom of the water column as a result of the weight of the water on top and is proportional to the depth of the water. The capillary pressure is a function of saturation (Figure 2.3). If the gas pressure is not sufficient, the pressure gradient in the flow equation (equation 2.6) is zero and no flow will occur. In low pressure gas distribution pipes the gas pressure is assumed to be 100 mbar, flow of gas can thus occur when the water and capillary pressure combined are less than 100 mbar (10.000 Pa).

With the following experiment it is determined at what water level gas can break through the column and the velocity with which the gas flows through the column is roughly estimated. In this Chapter the results are compared with the theory and later also with the numerical simulations.

6.1.1 Experimental set-up

The experimental set-up consists of a circular 90 cm long column with a diameter of 7 cm (Figure 6.1 a & b). The height of this set-up allows for similar pressures to occur as under field conditions. The small scale of the set-up limits the amount of unknown parameters. Seven centimeter from the bottom of the column there is a 5 mm wide inlet through which gas can flow into the column. A constant gas pressure is applied at this inlet using a gas pressure regulator connected to a gas pressure meter. An 8 mm wide tube filled with a small amount of water is situated between the pressure regulator and the inlet point which makes it possible to determine if any flow is passing through the column. At the bottom of the column the water pressure is measured using a water pressure gauge. There is also a transparent tube filled with water connected to the bottom of the column by a tap through which small amounts of water can be extracted and with which the water level can be regulated.

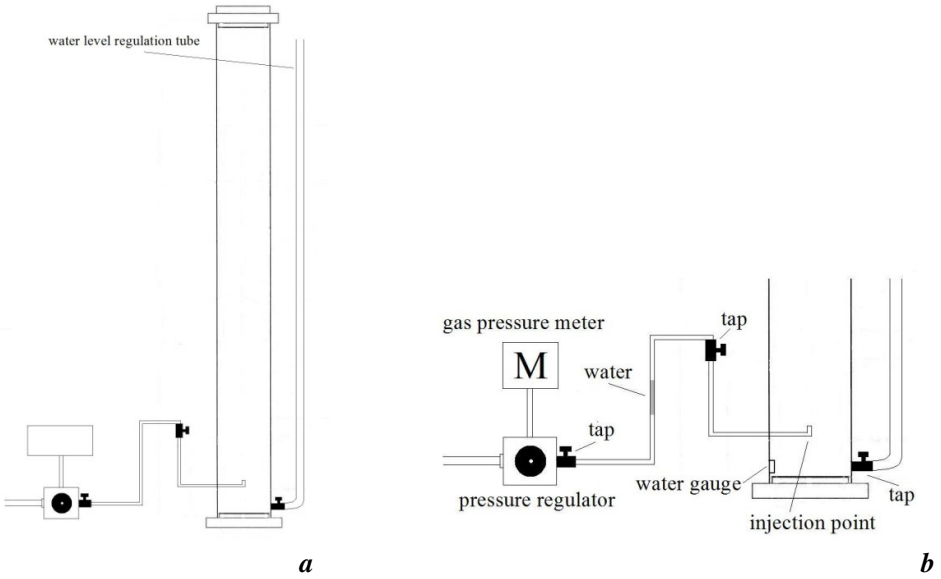

Figure 6.1 a) experimental set-up of the one-dimensional column experiment b) magnification of part of the set-up of the one-dimensional column experiment

6.1.2 Methods and materials

The column is half filled with degassed water, which prevents any air to accumulate between the grains. A 4 cm layer of very fine aluminum-oxide grains is inserted into the column. Next the sample material is slowly and continuously added while being tamped according to the Schenkeveld method (van der Poel & Schenkeveld, 1998), which results in a compact completely saturated soil of approximately 87 cm thick with a minimum porosity. The samples used are listed below in Table 6.1.

When the soil is completely compacted and saturated water is extracted from the column to decrease the water level. The very fine layer of aluminum-oxide will remain saturated throughout the entire experiment to make sure the water is not extracted from one point. The decreasing water level is measured using the pressure gauge and observed in the tube connected to the column. Lowering of the water level is a time consuming process, because water has to be extracted very slowly to prevent preferential flow paths to originate and to allow for equilibrium conditions to set in. When an equilibrium state is reached gas at a pressure of 100 mbar is applied to the inlet and a possible breakthrough is observed. This is repeated for several water levels. If a breakthrough occurs, the flow rate is approximated using the water movement in the water just above the pressure regulator. The flow is observed in the column and the time until the gas has reached the top of the column is recorded.

The experiment is conducted using Baskarp sand and glass beads (Table 6.1). Baskarp sand is used because it has a steep grain size distribution and much information is available on this sand (Appendix A). Glass beads are used because they have a small range in grain size distribution and are perfectly rounded, which makes it easier to prevent layering in this sample than in Baskarp sand.

Material	Grain size	d_{50}	Porosity
Glass beats	250 – 420 µm	335 µm	0.38
Baskarp sand	See appendix A	135 µm	0.36

Table 6.1 Description of samples used in the one-dimensional column experiment

Because the use of methane can cause a serious safety hazard and to make the experiments easier to conduct, in these experiments air is used as the gas phase instead of natural gas. Because air has a higher density than natural gas this may give a different result. But as stated before in Chapter 5 breakthrough is assumed to be similar for air and natural gas. The capillary pressure saturation curves are assumed to be similar for natural gas and air, since capillary pressure between water and gas phase is mainly determined by the fact that there are only few molecules in the gas phase. The difference in interaction of methane and air then has little effect (private communication with Prof. dr. ir. H. Bruining of the Delft University of Technology)
Because no quantitative results for the volumetric flow rate of the gas are measured differences in flow rate between air and natural gas are irrelevant.

6.1.3 Results

6.1.3.1 Baskarp sand
The first experiment is conducted over a time span of approximately six days. During this time the water pressure is measured by the water pressure gauge and the water level is observed in the water level regulation tube. This is displayed in Figure 6.2.

The water pressure measured by the pressure gauge generally correlates very well with the observed water level in water level regulation tube. Differences between the water pressure measured by the pressure gauge and the water level in the regulation tube are observed when gas pressure is applied. The water pressure in the pressure gauge rises as a result of the applied gas pressure

The first breakthrough of gas through the column is observed at a water level of 25 cm. This is approximately twenty hours after the start of the experiment. As a result of the gas entering the column the pressure gauge gives an increased water pressure, which is clearly visible in Figure 6.2. A very small gas inflow, too small to be measured, is observed for thirty minutes. After this the gas flow stagnates.

The water level is decreased and at 23 cm a breakthrough is again observed. A small gas inflow of approximately 1 ml/hour is observed for twenty minutes. After twenty minutes the gas flow stagnates again.
The water level is again decreased with steps of 1 cm and after every step a gas pressure of 100 mbar is applied. This can be seen in the enlarged section of the graph in Figure 6.2. Very

slow gas inflow is observed almost every step, but stagnates quickly after a few minutes. When the water level has reached a height of 14 cm above the inlet point a decrease in saturation is observed in the column at the level of the inflow point.

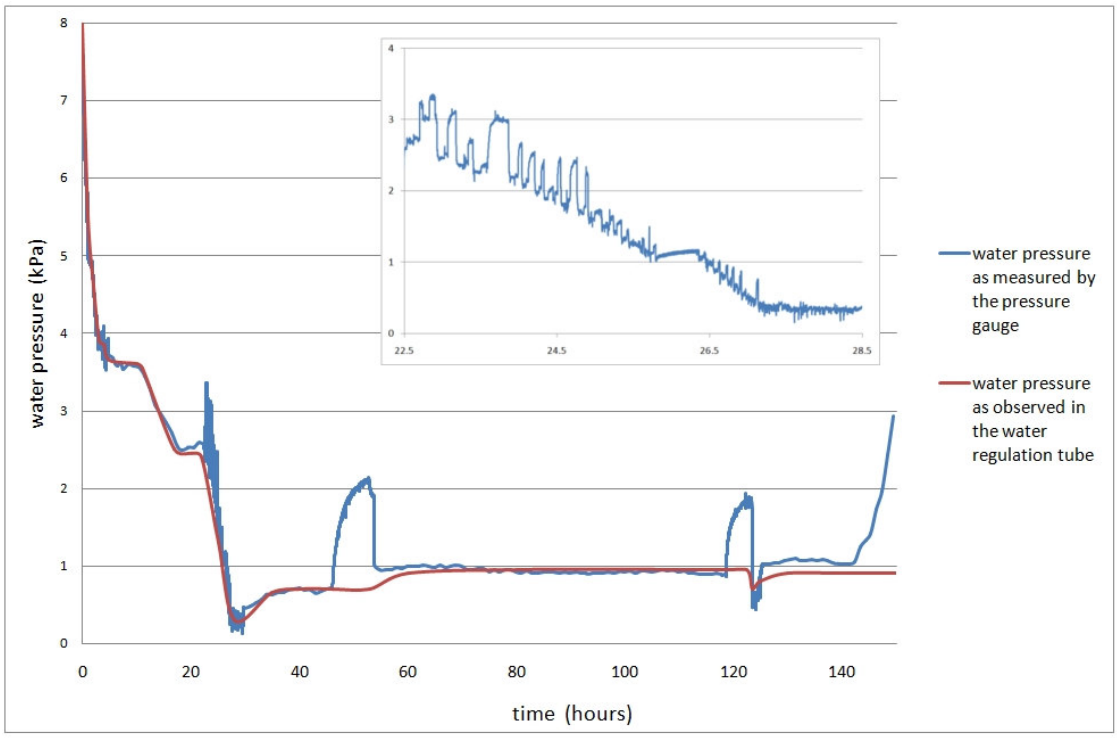

Figure 6.2 Water pressure as a function of time for the one-dimensional column experiment using Baskarp sand, measured by a pressure gauge and as observed in the water level regulation tube. An enlargement of the period from 22.5 hours to 28.5 hours is shown above the graph.

The lowering of the water level is continued. The water level is decreased to a minimum of 3 cm above the inlet. After approximately twelve hours the water level has risen from 3 cm to 8 cm, which indicates that equilibrium conditions have not been reached at 3 cm water level.

At a water level of 8 cm a gas pressure of 100 mbar is applied and a continuous flow of gas of approximately 0-3 ml/h is observed. After seven and a half hours no changes in flow rate are observed and the water level is again lowered to a water level of 7 cm.
After twenty hours the water pressure as measured by the pressure gauge as well as the water level in the water level regulation tube have both increased to give a water level of approximately 9.5 cm.

After approximately 118 hours, when the water level is 9,5 cm, gas at a pressure of 100 mbar is again applied and a continuous flow of gas of approximately 2.5 ml/h observed. The sand in the column starts to desaturate at the height of the inlet point. As a result of the continuous flow an increase in desaturation is observed higher in the column with time. Five hours after

the gas pressure is applied a decrease in saturation is visible up to a height of 20 cm above the inlet point. After seven hours desaturation is visible at the top of the column.

6.1.3.2 250-420 micron glass beads

The second experiment was conducted over a time span of seven weeks. During this time the water level is slowly decreased and water pressure is measured using a water pressure gauge. The water level as a function of time is displayed in Figure 6.3. As can be seen in the figure, the water pressure measured by the pressure gauge correlates very well with the observed water level in water level regulation tube.

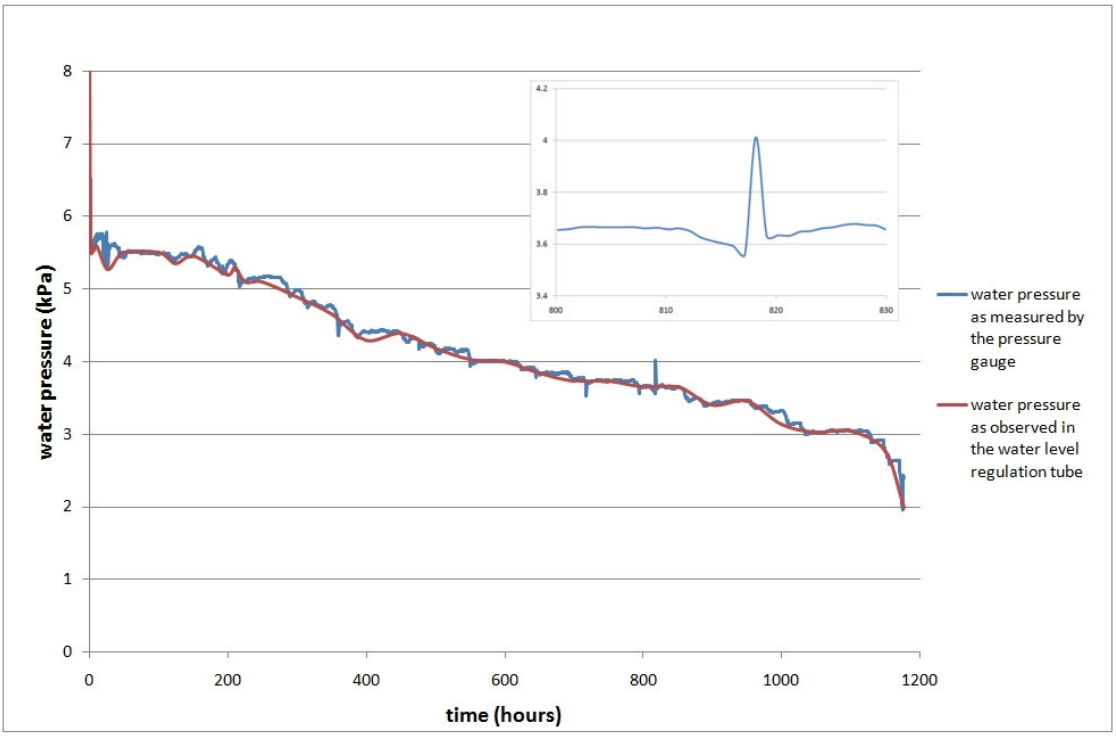

Figure 6.3 Water pressure as a function of time for the one-dimensional column experiment using 250-420 micron glass beads, measured by a pressure gauge and as observed in the water level regulation tube. An enlargement of the period from 800 hours to 830 hours is shown above the graph.

The first breakthrough of gas is observed at a water level of 36 cm, this is approximately 818 hours after the start of the experiment. A very small gas inflow in the range of 10-20 ml/h is observed for thirty minutes. As a result of the gas entering the column the pressure gauge gives an increased water pressure, which is clearly visible in the enlargement in Figure 6.3 where there is a small peak after approximately 818 hours. After thirty minutes the gas flow stagnates.

The water level is again decreased with steps of 1 cm and after every step a gas pressure of 100 mbar is applied. At a water level of 21 cm, there is again a breakthrough of gas. The rate with which the gas flows through the column is approximately 110-120 ml/h. This flow rate stays constant with time. Desaturation of the sample is visible at the side of the column. It

takes approximately thirteen minutes before the gas reaches the unsaturated zone of the column (21 cm above the inlet). The paths visible on the side of the column don't change with time and no new paths are formed.

6.1.4 Discussion and conclusions

In the experiment with glass beads, initial breakthrough occurs at a higher water level than in the experiment with Baskarp sand. This implies that Baskarp sand has a larger capillary pressure at the same saturation, which results in a higher entry pressure for the gas. This is probably due to the fact that the glass beads have a larger average grain size and probably even more important, a larger 15% size (d_{15}) of the grains. In general the capillary pressure is not assumed to be dependent on the average grain size, but on the d_{15} (private communication Deltares).

In both experiments the flow of gas stagnates after the first breakthrough. This could be due to several mechanisms. A possible explanation is, that when gas flows into the column it decreases the water saturation at the bottom of the column to a value lower than 99%. Water is then pushed upwards into the unsaturated zone which at the bottom of the unsaturated zone is nearly saturated, creating a saturated layer, and thus water pressure, which is larger than the water pressure at the start of the experiment. This water pressure will remain higher than the initial water pressure until equilibrium conditions are reached and the water pressure will again be equal to the initial water pressure.
The fact that water can only be pushed upwards is a side-effect caused by the size of the column. It is expected that in the field water will also flow sideward. Therefore, in the field the water pressure will not increase to the same amount. As a result of this, flow of gas will probably not stagnate in the field.
Another explanation for the stagnation of flow can be the formation of layering during filling of the column. This layering is more likely to occur in Baskarp sand than in glass beads due to the larger variability in grain size (Table 6.1 & Appendix A). Layering of different grain sizes results in layers with different capillary pressure and entry pressures. So when there is a saturated layer of very fine sand, water can always flow through this saturated layer, but if gas reaches this layer it may not be able to flow through due to the high capillary pressure of the fine layer. This can cause stagnation of flow.

The flow velocity of the gas is much lower in Baskarp sand than in the glass beads. This is a result of the larger average grain size and thus intrinsic permeability of the glass beads compared to Baskarp sand (Table 5.3, Bear 1972). The difference in flow velocity can also be influenced by the different shapes of the grains. Opposed to Baskarp sand, the glass beads are perfectly rounded, which can increase the permeability, and thus the flow velocity of the gas.

Another observation is that when a continuous flow of gas is established, no increase in velocity is observed during both experiments. This indicates that no new paths are formed during the flow of gas. This is also observed visually at the side of the column in the experiment with the glass beads. This could be a result of the size of the set-up. With a larger

set-up, gas could possibly have pushed the water sideways, resulting in less water at the top and thus a larger flow path with time.

These experiments suggest that breakthrough occurs at a higher water level in a sample with a larger d_{15}. This is also in concurrence with the theory. When a sample has a large variation in grain size and thus a relative small d_{15}, this could lead to a high capillary pressure and entry pressure. Flow velocity of gas is likely to increase with increasing grain size, but the shape of the grains might influence the flow velocity as well. The presence of layering could influence the flow of gas. Further study is necessary to get more insight.
Unfortunately the conducted experiments are very time-consuming, so only two experiments could be completed. It would be better if more experiments with different grain sizes could be conducted and if obtained results could be verified by conducting the same experiments multiple times. Although the experiments show some useful results, there are some uncertainties and recommendations, which can be taken into account for future experiments:

- The saturation cannot be determined in the column, which makes it uncertain if equilibrium conditions are reached. Therefore, it is unclear how fast water can be extracted from the column. Perhaps water has been extracted too fast, resulting in preferential paths of decreased saturation. This will have influence on the flow of gas through the column. It would be useful to measure the degree of saturation in the column previous to and during the flow of gas through the column. This could be done using TDR's, which can be placed in the column.

- The amount of gas flowing into the column is now roughly estimated. More detailed information about this flux would be useful.

- A large scale three-dimensional experimental set-up, where side-effects are limited, will be very useful for increasing the understanding of the flow of gas through the unsaturated zone.

6.2 One-dimensional column experiment with saturation and gas flow measurements

The experiment described above was adjusted to make it possible to measure saturation at six different points in the column and to measure the amount of gas flowing through. The amount of gas and the velocity of the flow can then be determined using the gas flow meter. Using the saturation measurements it will be possible to determine if equilibrium state is reached.

6.2.1 Experimental set-up

The experimental set-up is similar to the set-up used in the one-dimensional column experiment described in Section 6.1.1. The set-up consists of a circular 100 cm long column with a diameter of 9 cm (Figure 6.4). There is a 1 mm wide inlet through which gas can flow into the column at 11 cm from the bottom of the column.
A constant gas pressure is applied to this inlet using a pressure transducer connected to a gas pressure meter. A transparent tube filled with water is connected to the bottom of the column by a tap through which small l amounts of water can be extracted and with which the water level in the column can be determined.
The main difference between this setting and the setting used in the previous experiments is that there are six time domain reflectometers (TDR's) installed in the column which makes it possible to measure average saturation at six points in the column. They are situated 12 cm from each other starting approximately 10 cm above the injection point.
A gasflow meter, which can give a volume flux, is attached at the top of the column to measure the amount of gas flowing through the column.

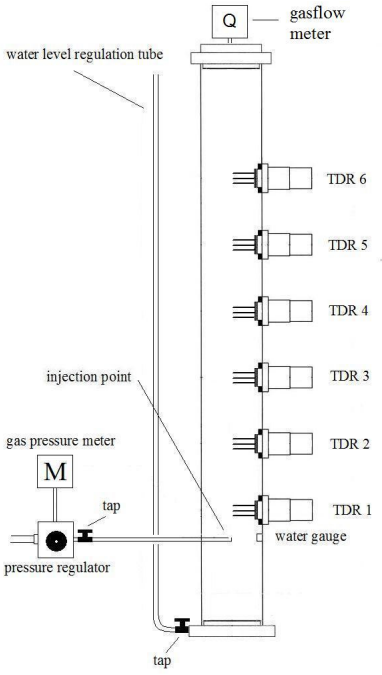

Figure 6.4 Experimental set-up for the one-dimensional column experiment with saturation and gas flow measurements

6.2.2 Methods and materials

The method used in this experiment is identical to the procedure described in Section 6.1.2. The only difference is that the compaction process needs to be carefully executed since there are TDR's in the column which should stay perfectly in place. Previous to the experiment the TDR's have been calibrated for Baskarp sand. This should improve the precision to 1% for the TDR measurements (Günzel et al., 2003).
After having created a compact, saturated soil with a minimum porosity of 36.1%, the water level in the column is decreased until equilibrium conditions are reached, which can now be determined using the TDR's and the water level regulation tube. Gas at a pressure of 100 mbar is then applied to the inlet. This is repeated for several water levels. If breakthrough occurs the amount of flow through the column is measured through time and the saturation of

the sample is measured at the six different points by the TDR's. As in the previous experiment, air is used as the gas phase.

Previous to the experiment the column is filled with completely dry Baskarp sand. When a pressure of 100 mbar is applied a volume flux of 4.3 l/hour is measured. It has to be kept in mind that no minimum porosity is obtained when filling the column with completely dry sand, which may increase the permeability and thus the flow rate of the gas through the column.

6.2.3 Results

The experiment was conducted over a time span of six weeks. During this time the water level is slowly decreased and water content is measured by the TDR's placed in the column.
The water content as a function of time is displayed in Figure 6.5. The calculated porosity of the sample is 0.36. The TDR's measure a water content of approximately 38% indicating a porosity of 0.38. This difference could be due to the fact that it is hard to solidify the sample near the TDR's, which will lead to a higher porosity near the TDR's.

The first breakthrough of gas occurs at a water level of 16 cm. At this point drying is observed around the inlet point, but no flux of gas is observed. At a water level of 12 cm a small flux of gas of approximately 1 ml/h is observed. The flow of gas stagnates after 45 minutes. No change in saturation is measured by the TDR's.

The water level is decreased with steps of 1 cm and after every step a gas pressure of 100 mbar is applied. Very slow gas inflow is observed almost every step, but decrease with time. The initial volume fluxes of gas flowing through the column are measured and given as a function of water level in Figure 6.6. Every time step gas is applied for approximately two days. At these water levels no significant change in saturation is observed when lowering the water level or when gas flow through the column.

When the water level is 9 cm above the inlet, a gas pressure is again applied and a decrease in saturation of the sample is observed by the lower three TDR's after approximately two days (Figure 6.5). TDR one give a change in saturation of ± 1.5% over the entire area. Because the sample has an average porosity of ± 38%, this corresponds to a change of saturation of 4.0%. TDR's two and three give a change in saturation of ± 3 % over the entire area which corresponds to a change in saturation of 7.9%. This is visible in Figure 6.6 after approximately $2.2 \cdot 10^6$ seconds. After another four days, when time is $2.76 \cdot 10^6$ seconds, no more flow is observed and the water level is lowered to 8 cm.

At $2.78 \cdot 10^6$ seconds, at a water level of 8 cm, gas pressure of 100 mbar is applied. After five hours and thirty minutes, at a time of $2.8 \cdot 10^6$ seconds, desaturation of the sample near TDR five and six is measured. TDR five gives a change in saturation of ± 4% over the entire area,

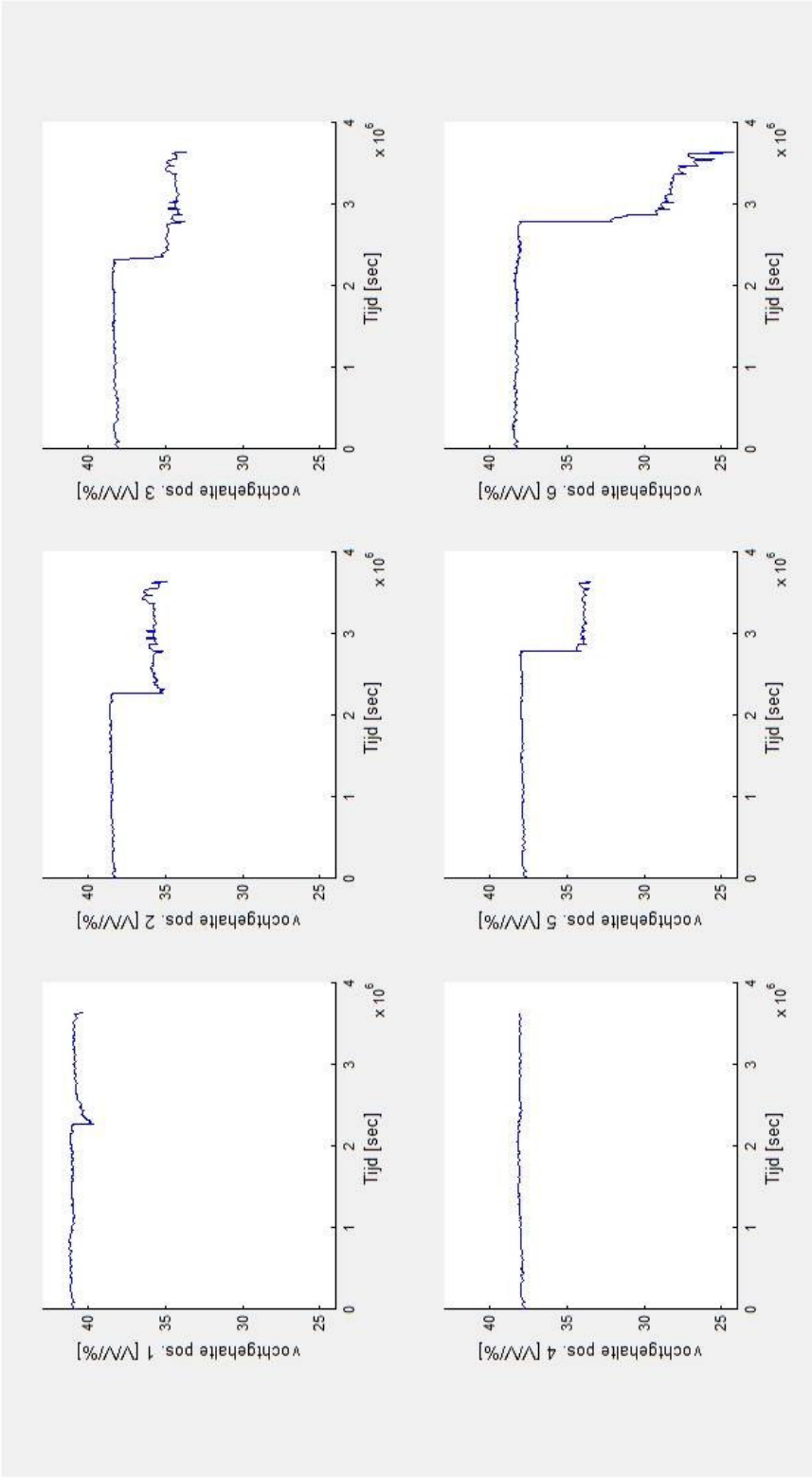

Figure 6.5 Degree of saturation measured as a function of time by six time domain reflectometers placed in a column at different heights for a one-dimensional gas flow simulation experiment.

which corresponds to a change in saturation of 10.5%. TDR six gives a change in saturation of ± 6% over the entire area, which corresponds to a change in saturation of 15.8%. No change in saturation near TDR four is observed. The measured flow of gas decreases with time.

The water level is again decreased. While lowering a decrease in saturation near TDR six is observed and an increase in saturation near the other TDR's is observed. TDR one gives the largest increase in saturation (Figure 6.5). When equilibrium conditions have been met, a gas pressure is applied and the volume flux of gas is measured. As can be seen in Figure 6.6, the initial values for the volume flux of gas increase with decreasing water level, with a maximum value of 190 ml/hour observed at a water level of -5 cm. This volume flux is more than one hundred times smaller than the maximum flux measured in dry Baskarp sand previous to the experiment.

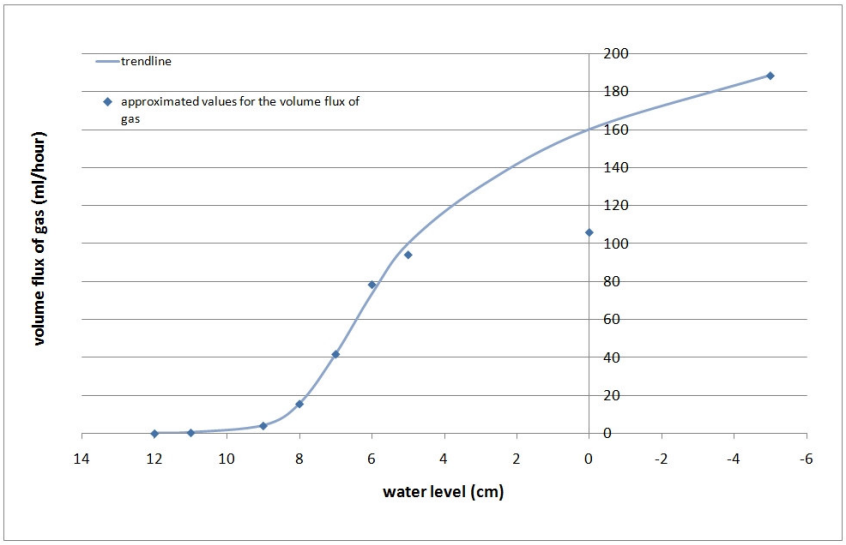

Figure 6.6 Approximated values for the initial volume flux of gas as a function of water level.

6.2.4 Discussion and conclusions

It appears that the volume flux of gas flowing through the column increases with decreasing water level. The flow can vary from a few milliliters per hour in almost saturated sand to approximately four liters per hour in completely dry sand. However no quantitative estimates about the change of the volume flux with water level can be made from this experiment. This is because after the first breakthrough of gas unsaturated flow paths occur. These flow paths cannot become completely saturated again and will therefore influence the ease with which gas can flow through the column. To make correct estimates of the volume flux, for each water level a new experiment would have to be conducted.
Another problem is the size of the volume flux, which is very small and difficult to measure. More accurate measurements will increase the reliability of the experiment.

Just as in the previous experiments a decrease and sometimes even stagnation of the volume flux with time is observed. This is probably due to side-effects caused by the size of the column. The mechanisms that could have caused this decrease in velocity or stagnation are the same as suggested in the previous experiment.

Desaturation of the column as a result of lowering of the water level is only observed in TDR six at a water level of 9 cm. The fact that no change in saturation is measured by the other TDR's is probably because of the high entry pressure of Baskarp sand, which must be approximately 65 cm. This high entry pressure results in a minimum change in saturation in the 65 cm above the inlet point which will thus remain almost completely saturated.

The maximum decrease of saturation due to the inflow of gas is in the range of approximately 4 to 15%. This could be due to the formation of flow paths in the column. The increase of desaturation with increasing height could indicate a cone shaped pattern of flow paths. The fact that there is no change in saturation measured near TDR four also indicated the formation of flow paths. Because the TDR's only measure the average saturation in between the pins a flow path could have formed alongside the TDR, leaving the area measured by the TDR completely saturated.

No clear relation between the volume flux of gas flowing out of the column and saturation can be found. Because the flow velocity is dependent on the relative permeability of the gas which will increase with decreasing saturation, an increase of volume flux with decreasing saturation is expected. As mentioned above there seems to be a relationship between volume flux and water level. Because the degree of saturation in the column is dependent on the water level, a relation between volume flux and saturation is expected. Perhaps the changes in saturation are too small to be measured. The decrease in saturation as a result of the inflow of gas could also give a distorted view on the variation in saturation.

From this experiment it can be concluded that a decrease in water level seems to lead to an increase in volume flux of gas measured at the top of the column, but that no quantitative estimates about the variation of volume flux with water level can be made. A dependency of flow velocity of gas with saturation is expected. As expected, the flow velocity in dry Baskarp sand is much higher than in a partly saturated Baskarp sand. Although the volume flux seems to increase with decreasing water level, only one clear decrease in saturation is observed.

Just as in the previous experiments, this experiment is very time-consuming, but to make correct estimates of the volume flux a new experiment would have to be conducted for every water level. Because there are still some uncertainties and side-effects, recommendations, which can be taken into account for future experiments are:

- The result would also improve with more accurate measurements of volume flux of gas flowing out of the column.
- Although difficult to obtain saturation values for the entire cross-section of the column would be useful.

- To minimize the side-effects which are expected to influence the results, large scale experiments should be conducted. Such an experiment will however be very hard to conduct. It will be necessary to have complete knowledge of the degree of saturation in the set-up. This will be very difficult in a larger set-up. Extraction of the water from the bottom could also be problematic in a large scale set-up. Just as the experiments described above it will be a very time-consuming experiment.

6.3 Two-dimensional preferential flow path experiment

When a wetting front advances through an unsaturated soil, soil heterogeneities can lead to distinct fingering phenomena (Conciani et al., 1995). In the case of gas leaking from a low pressure distribution pipe the process is not the same, since it is a non-wetting front that is forced through an initially saturated or unsaturated soil at a constant pressure of 100 mbar. Although the process is not the same similar phenomena can be expected. In both cases it is expected that high permeability paths within the soil control the advance of either a wetting or a non-wetting front.

To get a better understanding of the influences of soil heterogeneity on the flow of gas several experiments are conducted. For these experiments a two-dimensional set-up is designed which makes it possible to visualize the preferential flow paths behind a perspex plate. Results of these experiments will later be compared with the numerical simulation.

6.3.1 Experimental set-up

The experimental set-up consists of a rectangular shaped flat tank with a width of 42 cm, a height of 30 cm and a depth of 5 cm (Figure 6.7). At the bottom of the tank there is a 1 mm wide slid through which the gas can enter the tank and 4 holes which can be used for dewatering.

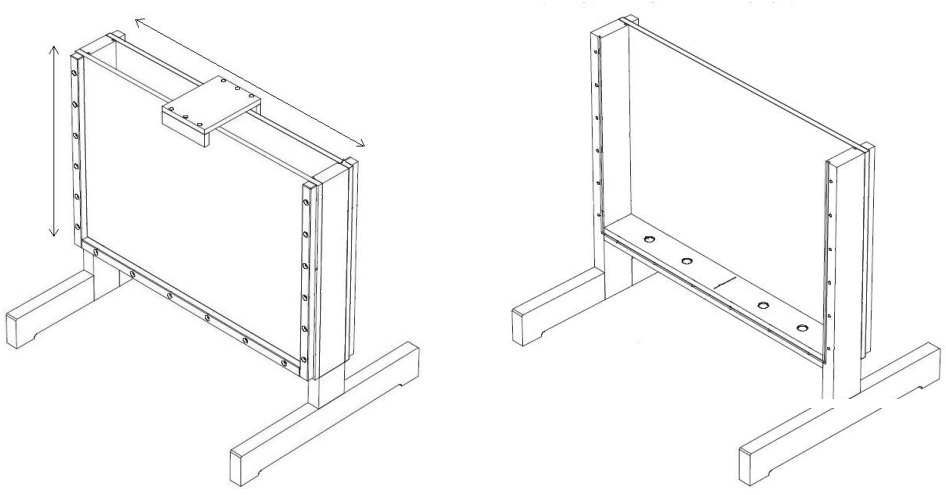

a. ***b.***

Figure 6.7 a) experimental set-up 2-D experiment. b) experimental set-up when opened.

6.3.2 Methods and materials

The tank is filled with degassed water to which sand or glass beads are slowly and continuously added while being tamped into a compact completely saturated soil of approximately 25 cm thick with a minimum porosity. To make sure that it is not possible for gas to displace any glass beads or sand grains, a metal filter is placed upon the sample. Upon

this filter weights are applied which make it possible for water and gas to move through, but makes sure that the glass beats remain in place creating an undeformable soil skeleton.
By completely filling the slid with geotextile, which allows air to flow through, the air is forced into the slid before entering the soil creating a line source of gas. When the soil is completely compacted and saturated a pressure is applied at the inlet. The decrease in saturation which is a result of the flow of gas is visualized through the perspex plate.

Ten different experiments are conducted multiple times with two different types of materials; glass beads of three varying grain sizes and Baskarp sand (appendix A) (Table 6.2). In the first experiments the tank is filled with one material, in later experiments layers of a different material or grain size are created. The pressure also varies between experiments. First the applied pressure is just large enough to overcome the capillary pressure and water pressure to cause a breakthrough. When steady state is reached, the pressure is then increased to 100 mbar. In the following experiments a constant gas pressure of 100 mbar is applied during the whole experiment. The criteria used for steady state is that the width of visible desaturation of the soil, and thus the width of the spreading of the gas, remains stable over a period of one day.
The conducted experiments are listed in Table 6.2. Some experiments were conducted multiple times for verification.

Material	**Grain size**	**Porosity**	**Applied pressure**
Glass beads	149 – 250 µm	0.38 ±0.02	90 mbar – 100 mbar
“ ”	250 – 420 µm	0.36 ± 0.02	90 mbar – 100 mbar
“ “	420 – 840 µm	0.34 ± 0.02	90 – 100 mbar
“ “	149-420 µm	0.37 ± 0.03	90 – 100 mbar
“ “	149-840 µm	0.36 ±0.03	90-100 mbar
Baskarp sand	see appendix A	0.36 ± 0.02	100 mbar
Glass beads	420-840 µm with 149-250 µm layers	0.34 ±0.02 0.38 ± 0.02	90 mbar - 100 mbar
" “	250-420 µm with 149-250 µm layers	0.36 ± 0.02 0.38 ± 0.02	90 mbar - 100 mbar 100 mbar
“ “	149-250 µm with 420-840 µm layers	0.38 ± 0.02 0.34 ± 0.02	100 mbar
Baskarp sand & glass beads	Baskarp sand with 420-840 µm layers	0.36 ± 0.02 0.34 ± 0.02	100 mbar

Table 6.2 Description of samples used in the two-dimensional preferential flow path experiment.

6.3.3 Results

6.3.3.1 Uniform sample of 149-250 micron glass beads

In the first experiment gas can enter the tank at a minimum pressure of 80 mbar. After thirty minutes a steady state situation is reached and three preferential flow paths with a total width of approximately 14 cm are visible on the glass plate (Figure 6.8a). After this the pressure is increased to 100 mbar. A new path is formed and the existing two paths are widened, creating a V-shaped pattern. The pattern has a maximum width of approximately 20 cm (Figure 6.8b). A repetition of the experiment gave very similar results.

In a second experiment a constant pressure of 100 mbar is applied. One relatively straight path becomes visible on the glass plate which widens with time. After ten minutes it has formed a 11 cm wide path (Figure 6.9). After this, no new paths are formed. The main difference between this result and the results of the experiments starting with a pressure of 80 mbar is that now there are no separate preferential paths visible on the glass plate.

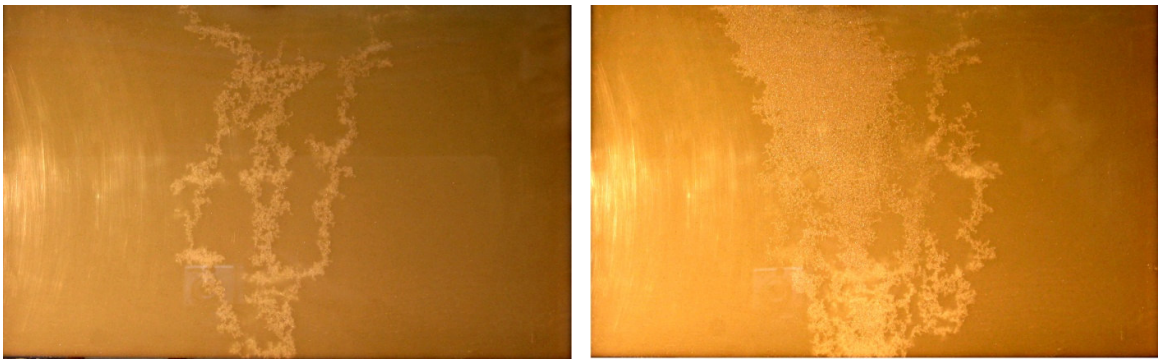

a *b*

Figure 6.8 a) Gas flows through the sample at a constant pressure of 80 mbar, picture is taken at steady state conditions, b) after this the pressure is increased to 100 mbar, picture is taken at steady state conditions

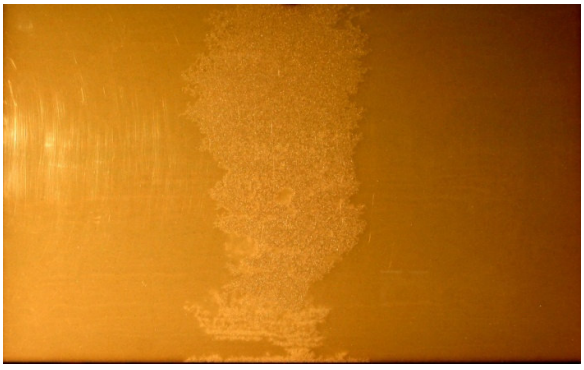

Figure 6.9) gas applied at a constant pressure of 100 mbar, picture taken after 10 minutes when steady state conditions are reached

6.3.3.2. Uniform sample of 250-420 micron glass beads

In the first experiments a constant pressure of 90 mbar is applied until a steady state situation is reached (Figure 6.10a). There are 4 preferential flow paths visible on the glass plate of which the three on the right are braided to form a small network with a maximum spreading width of approximately 10 cm. Then, pressure is increased to 100 mbar and a branching of the existing flow paths into a wider V-shaped network of preferential paths occurs (Figure 6.10b). The width of the V-shape is approximately 18 cm at the top.

In the last two experiments a constant pressure of 100 mbar is applied. A V-shaped network of small preferential paths is visible on the glass plate (Figure 6.11). In the first experiment the V-shaped network has a width of 16 cm at the top, in the second experiment the width is 20 cm at the top.

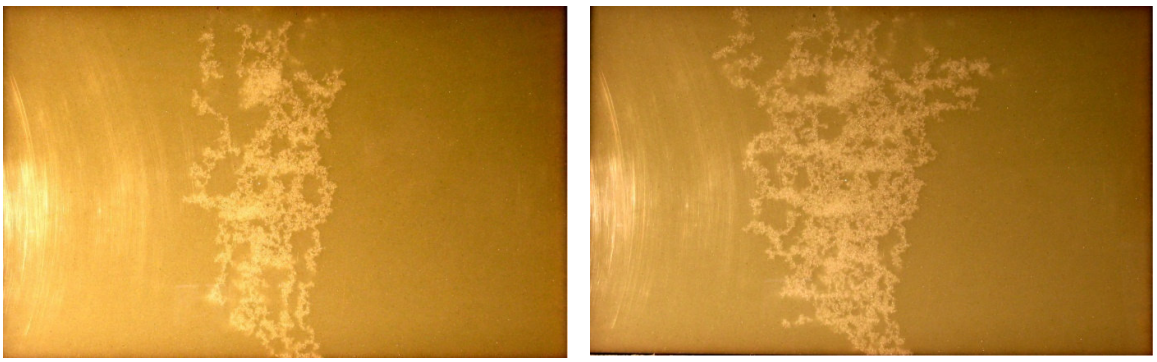

a *b*

Figure 6.10 Gas is applied at a constant pressure of 90 mbar, picture is taken after a) 15 minutes, when a steady state has been reached. b) The pressure is then increased to 100 mbar, picture is taken at steady state conditions

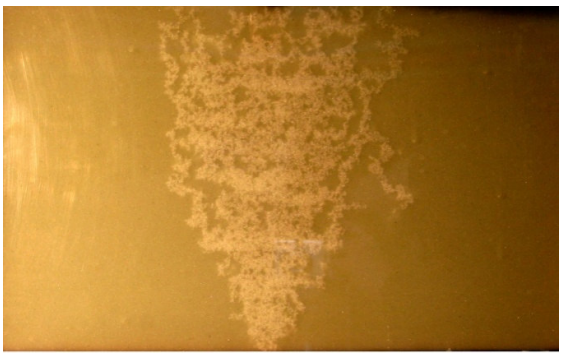

Figure 6.11 Gas is applied at a constant pressure of 100 mbar, picture is taken at steady state conditions

6.3.3.3 Uniform sample of 420-840 micron glass beads

In the first experiment gas is applied at a constant pressure of 85 mbar. One preferential path originates at the bottom of the tank. At the top 5 cm of this path branching occurs (Figure 6.12a). Steady state is reached after one hour, the gas pressure is increased to 100 mbar after 18 hours. As a result of increased pressure two additional flow paths originate which become branched forming a V-shaped network (Figure 6.12b). The maximum width of the V-shape is approximately 16 cm.

In another experiment a constant pressure of 100 mbar is applied. Air starts flowing in immediately and flows almost straight up to reach the top of the tank in twenty seconds (Figure 6.13). After this, no new paths are formed.

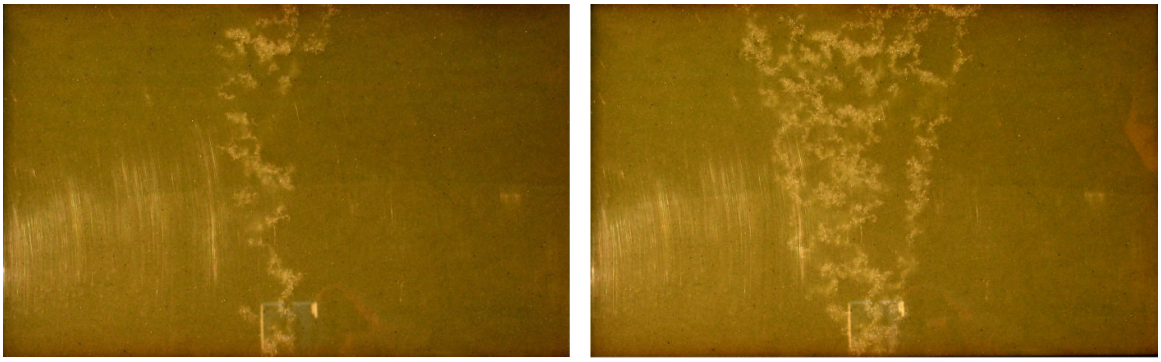

a *b*

Figure 6.12 Gas is applied at a constant pressure of 85 mbar, a picture is taken after a) 18 hours when a steady state situation is reached b).Pressure is then increased to 100 mbar, picture is taken at steady state conditions.

Figure 6.13 Gas is applied at a constant pressure of 100 mbar, picture is taken at steady state conditions.

6.3.3.4 Uniform sample of 149-420 micron glass beads

In the first experiment a gas pressure of 90 mbar is applied. The sample is not completely uniform but shows some layering. When the air flows in, two big paths are formed. The left path consists of smaller paths that are braided. It is clearly visible that the air follows the horizontal layering. When steady state is reached (Figure 6.14a), gas pressure is increased to 100 mbar. The existing paths are widened and the air spreads over the bottom layer until it reaches the edge of the tank (Figure 6.14b).

In the second experiment a constant gas pressure of 100 mbar is applied. This sample shows less layering then in the previous experiment. After applying pressure a V-shaped pattern of four main branches forms on the glass plate (Figure 6.15). The maximum width of the spreading visible on the glass plate is approximately 21 cm. Not visible here is the desaturation that is observed at the side of the tank, which indicates a much wider spreading.

a *b*

Figure 6.14 Gas is applied at a constant pressure of 90 mbar, b) the pressure is increased to 100 mbar, steady state situation

Figure 6.15 Gas is applied at a constant pressure of 100 mbar.

6.3.3.5 Uniform sample of 149-840 micron glass beads

Breakthrough of gas was observed at a minimum gas pressure of 90 mbar. This gas pressure results in a V-shaped pattern of braided paths (Figure 6.16a). The width of this pattern is approximately 23 cm at the top. When steady state is reached, the pressure is increased to 100 mbar. As a result, some small new paths are formed and some paths are a bit widened (Figure 6.16b).

In the second experiment a constant pressure of 100 mbar is applied. When air is flowing in, a V-shaped pattern is formed consisting of many small braided paths. There are no large preferential paths visible. When steady state is reached (Figure 6.17), air is flowing out over a width of approximately 24 cm.

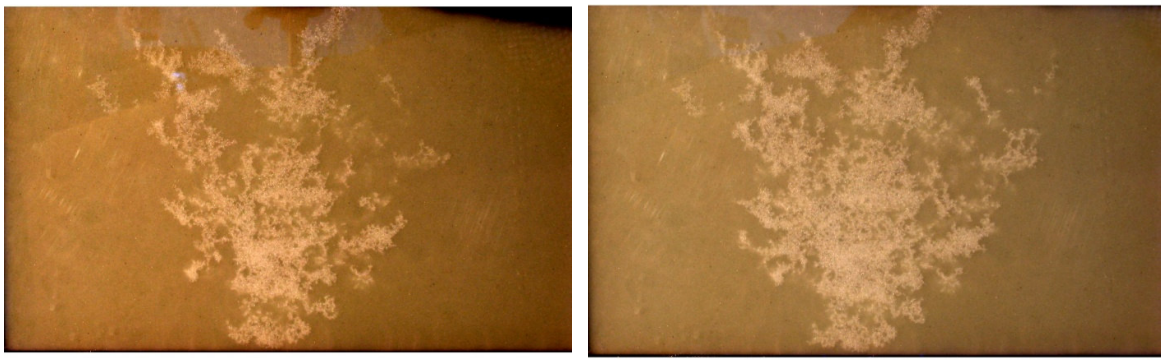

a b

Figure 6.16 a) steady state conditions as a result of a gas pressure of 90 mbar b) steady state conditions after increasing the pressure to 100 mbar

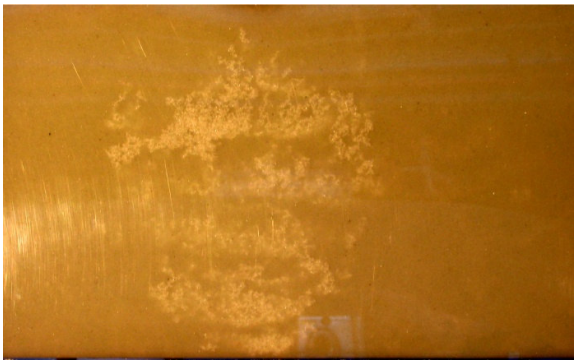

Figure 6.17 149-840 micron glass beads at a gas pressure of 100 mbar at steady state conditions

6.3.3.6 Baskarp sand

During filling of the tank, a thin layering caused by grain size differences is visible. When a pressure of 100 mbar is applied, gas slowly flows into the sample, spreading through these thin layers reaching a maximum width of 27 cm. Slowly, the gas flows to higher layers and spreads horizontally in these layers as well. The width of the spreading decreases width height. After twenty minutes, when the pattern has reached a height of approximately 6 cm on the glass plate, gas bubbles are visible on top of the sample. The flow path going to the top is not visible on the glass plate. The experiment was conducted multiple times with similar results.

6.3.3.7 420-840 micron glass beads with 3 layers of 150-250 micron glass beads

A gas pressure of 90 mbar is applied to the sample. The gas flows in and accumulates under the layer of 150-250 micron glass beads (Figure 6.18a). After three minutes the gas breaks through the layer to accumulate under the second layer (Figure 6.18b & c). The point where the gas breaks through is not visible on the glass plate. After 6 minutes it finds a path around the second layer and now starts to accumulate under the third layer (Figure 6.18d). After ten minutes the gas finds a path around the third layer and reaches the top. No significant changes are observed after this, which implies that steady state is reached (Figure 6.18e). Pressure is increased to 100 mbar and more gas accumulates under all three layers (Figure 6.18f). The same thing happens when the gas pressure is again increased to 110 mbar and 125 mbar (Figure 6.18g & h).

6.3.3.8 250-420 micron glass beads with 3 layers of 149-250 micron glass beads

For the first forty minutes a constant pressure of 85 mbar is applied. The gas accumulates under the first layer, but then stops to flow. The pressure is then increased to 90 mbar. More gas accumulates under the first layer (Figure 6.19a). After one hour and five minutes the gas breaks through the first layer at one point and starts to accumulate under the second layer (Figure 6.19b). One minute after this there is a second point in the first layer where the gas breaks through (Figure 6.19c). Nine minutes later the gas finds a path around the second layer to accumulate under the third layer (Figure 6.19d). After one hour and twenty minutes the gas flows around the third layer and reaches the top. Two hours after the start of the experiment a steady state situation is reached (Figure 6.19e). The pressure is then increased to 100 mbar. One and a half minute after increasing the pressure there are three new points through which gas breaks through the first layer and more gas accumulates under the second layer (Figure 6.19f). In the steady state situation more gas accumulates under the layers as a result of increased pressure and the paths around the second and third layer become wider (Figure 6.19g).

6.3.3.9 149-250 micron glass beads with 3 layers of 420-840 micron glass beads

Gas is applied at a constant pressure of 100 mbar which forms a 3 cm wide straight network of preferential flow paths through the 150-250 micron layer into the 425- 850 micron layer (Figure 6.20a). After entering the first layer the gas spreads horizontally until the first layer is completely filled, this takes six minutes (Figure 6.20b). After approximately six and a half

minutes the gas starts flowing out over the whole width of the first layer (Figure 6.20c). It forms a 10 cm wide straight network through the 150-250 μm glass beads to the second layer (Figure 6.20d). There it again pushes all the water out of the layer until it is unsaturated and starts to flow out (Figure 6.20e). This happens after approximately fifteen minutes. The gas then flows from the second to the third layer through a thirty centimeter wide network of small flow paths. After twenty minutes all the water is pushed out of the third layer and air is observed to reach the top of the tank (Figure 6.20f). Eventually all the layers are completely unsaturated and the gas in the 150-250 micron grains gives a V-shaped network of small flow paths (Figure 6.20g)

6.3.3.10 Baskarp sand with layers of 250-420 micron glass beads

After applying a constant pressure of 100 mbar gas slowly enters the tank. The gas seems to flow through thin layers which originated during filling of the tank. The width of the spreading of the gas visible on the glass plate is approximately 15 cm. After thirty minutes it reaches the first layer (Figure 6.21a). When the gas enters the first layer the flow rate of the gas increases and the gas starts spreading over the layer until it seems to be completely unsaturated (Figure 6.21 b & c). This is after two hours and thirty minutes. Two minutes later gas enters the second layer of glass beads (Figure 6.21d). No flow path of gas through the layer of Baskarp sand is visible on the glass plate. The gas spreads until the second layer seems to be completely unsaturated (Figure 6.21e). After approximately three hours gas quickly flows into the third layer. A 7 cm wide network of small flow paths is visible in the layer of Baskarp sand. It is not visible on the glass plate whether it is in contact with the third layer (Figure 6.21f). Water is quickly pushed out of the third layer by the gas. After three hours and fifteen minutes the third layer seems to be completely unsaturated and gas bubbles are visible on top of the sample. Flow paths to where the gas reaches the top of the sample are not visible on the glass plate (Figure 6.21g).

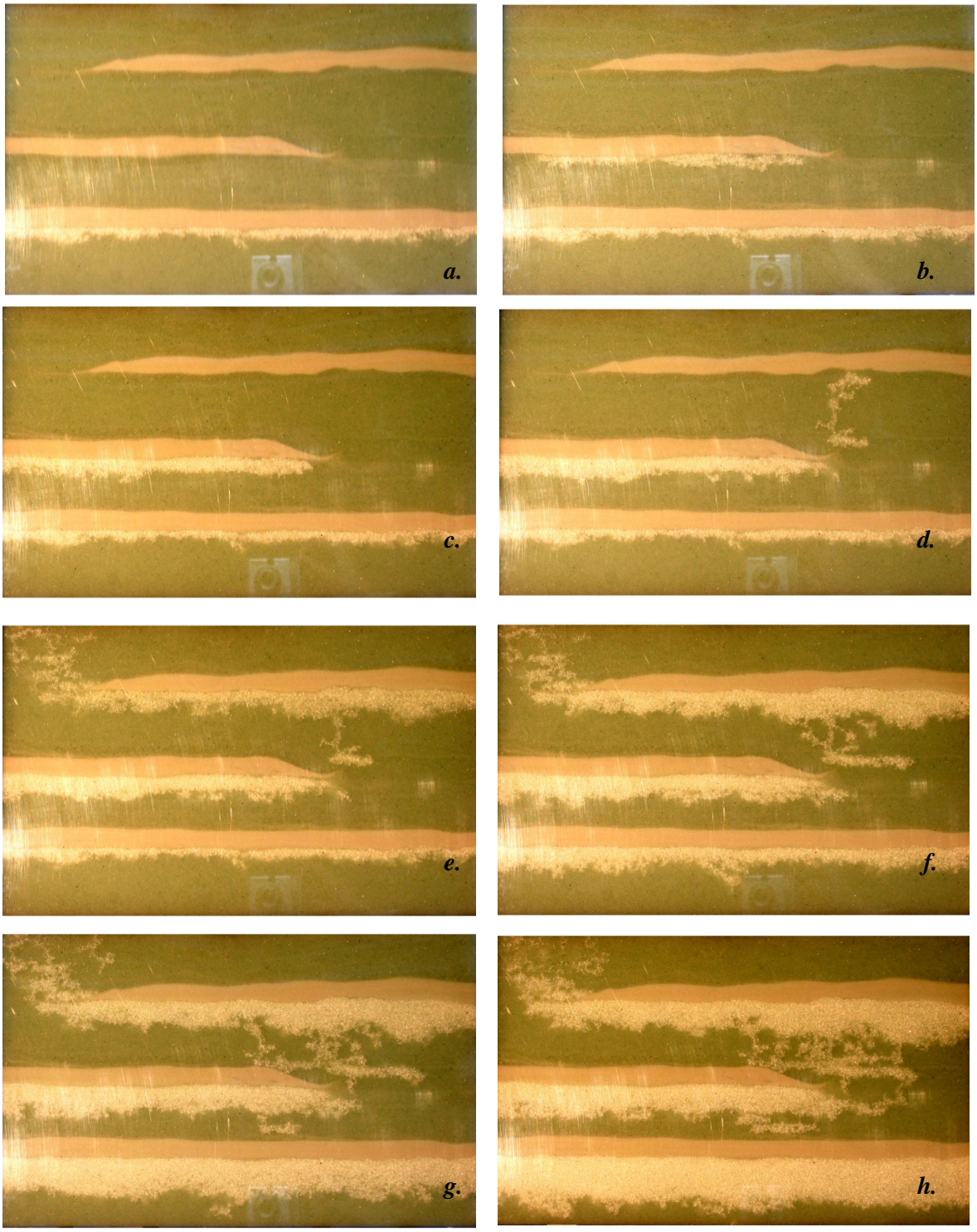

Figure 6.18 420-840 micron glass beads with layers of 149-250 micron. First a pressure of 90 mbar is applied. Pictures were taken after: a) 2 minutes, b) 3 minutes, c) 5 minutes, d) 6 minutes, e) 25 minutes, Then the pressure was increased to 100 mbar, pictures were taken after: f) 10 minutes (steady state). The pressure was again increased to g)110 mbar and h)125 mbar.

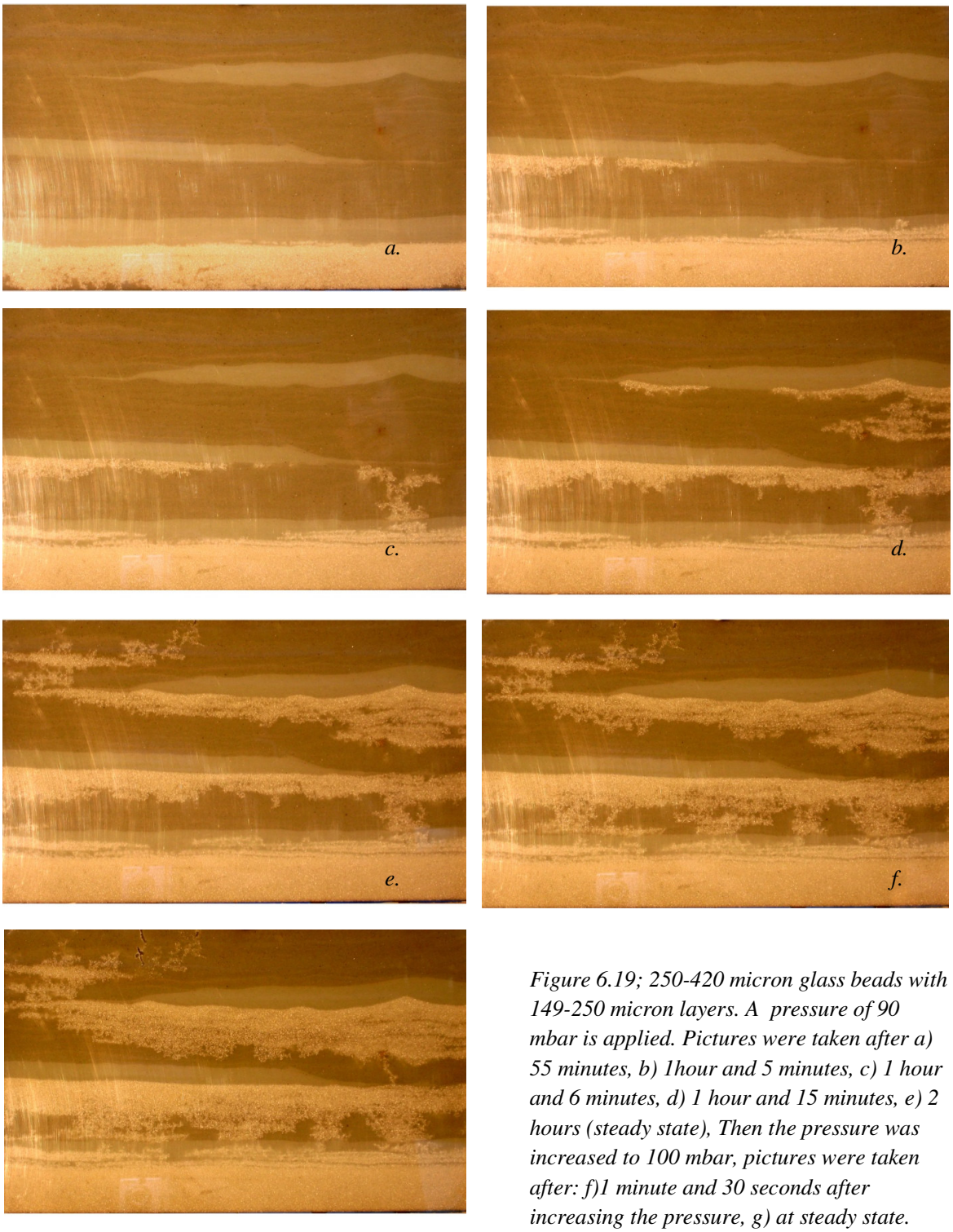

Figure 6.19; 250-420 micron glass beads with 149-250 micron layers. A pressure of 90 mbar is applied. Pictures were taken after a) 55 minutes, b) 1hour and 5 minutes, c) 1 hour and 6 minutes, d) 1 hour and 15 minutes, e) 2 hours (steady state), Then the pressure was increased to 100 mbar, pictures were taken after: f)1 minute and 30 seconds after increasing the pressure, g) at steady state.

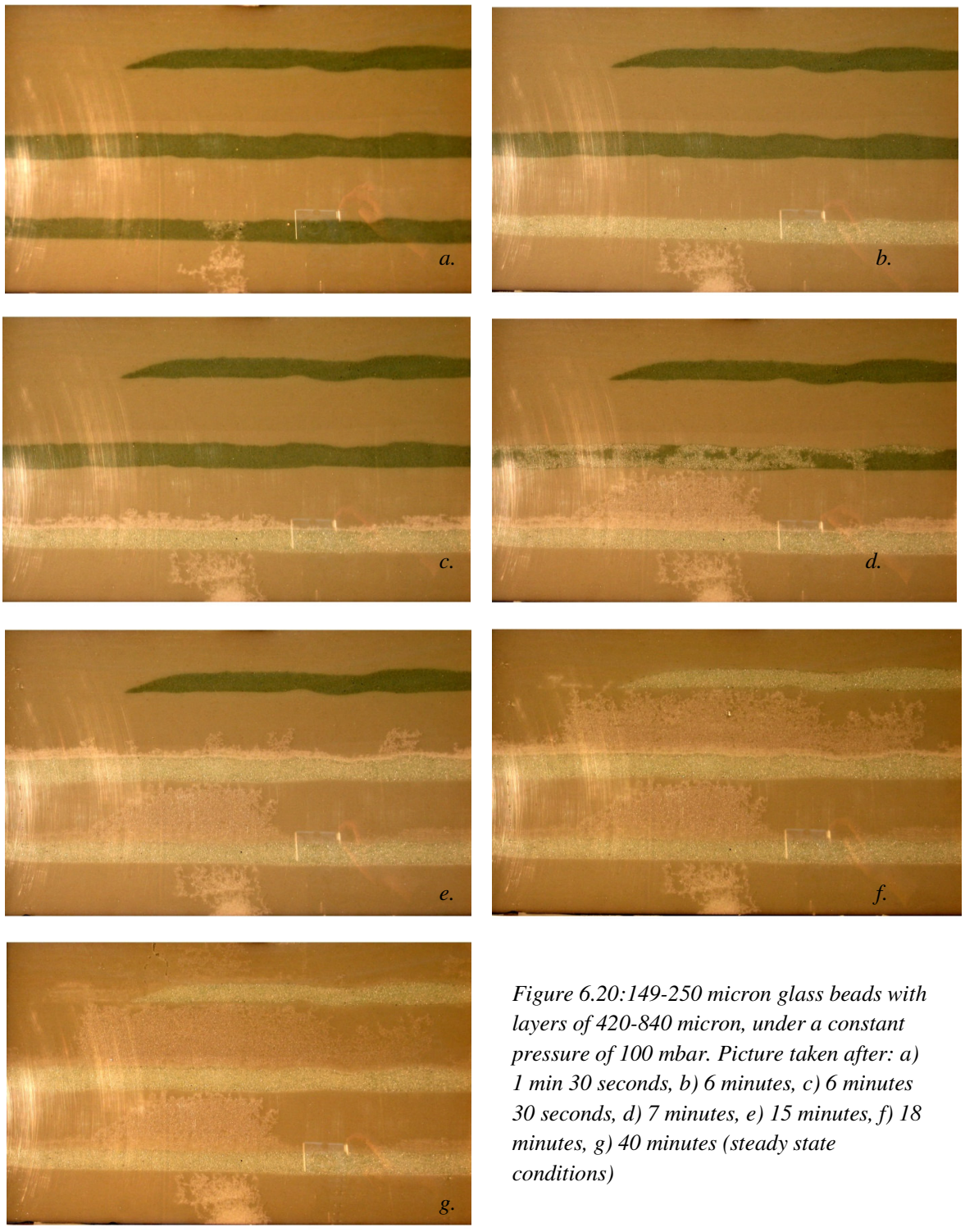

Figure 6.20:149-250 micron glass beads with layers of 420-840 micron, under a constant pressure of 100 mbar. Picture taken after: a) 1 min 30 seconds, b) 6 minutes, c) 6 minutes 30 seconds, d) 7 minutes, e) 15 minutes, f) 18 minutes, g) 40 minutes (steady state conditions)

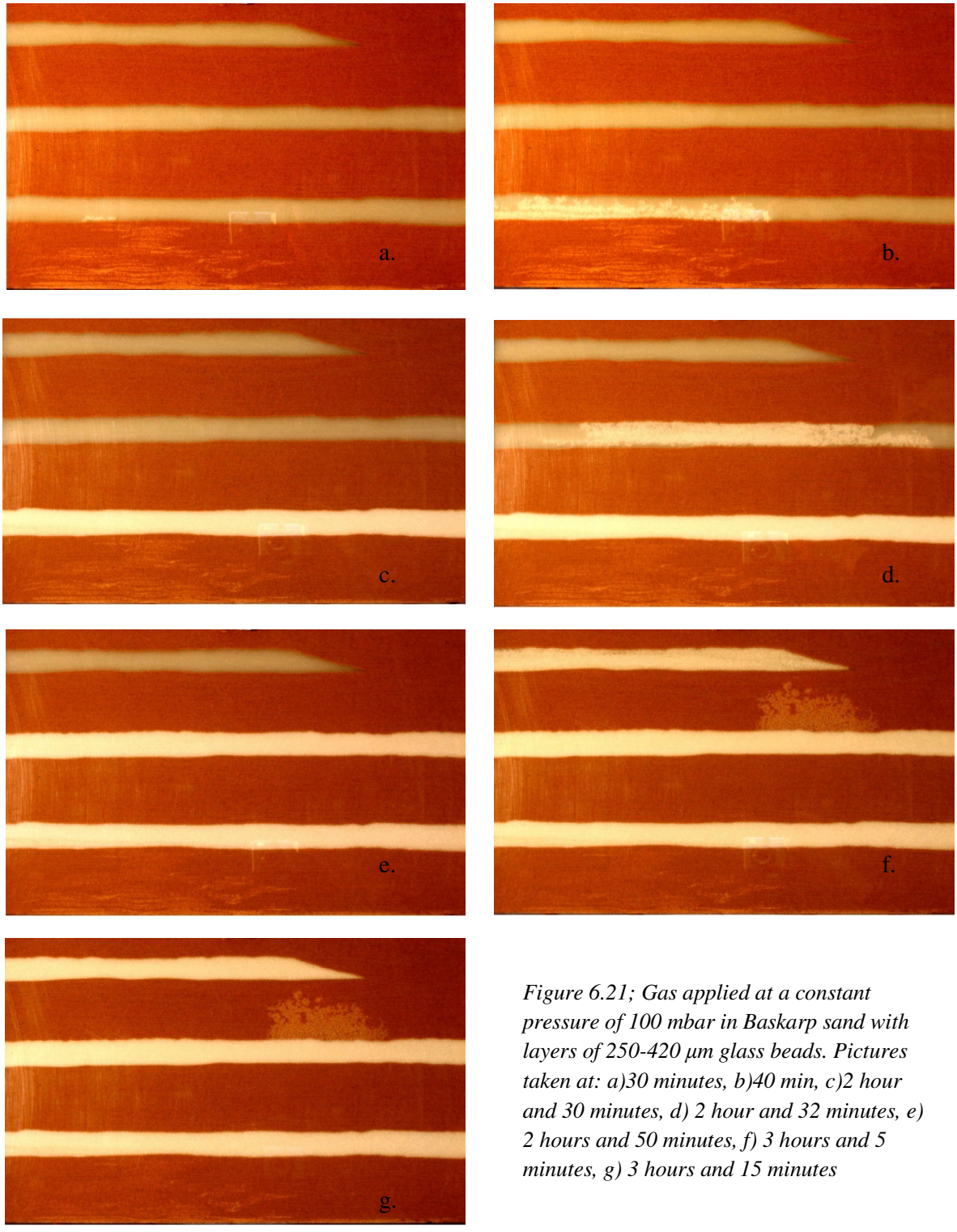

Figure 6.21; Gas applied at a constant pressure of 100 mbar in Baskarp sand with layers of 250-420 µm glass beads. Pictures taken at: a)30 minutes, b)40 min, c)2 hour and 30 minutes, d) 2 hour and 32 minutes, e) 2 hours and 50 minutes, f) 3 hours and 5 minutes, g) 3 hours and 15 minutes

6.3.4 Discussion and conclusions

When looking at the spreading width of the gas in experiments 6.3.3.1, 6.3.3.2 and 6.3.3.3, there is a small decrease of width with increasing grain size. The differences are small and could be due to the different grain size distribution ranges of the samples as well as to different grain sizes. To verify whether the grain size distribution range influences the spreading width, experiments with larger ranges have been conducted (6.3.3.4 and 6.3.3.5). As a result of the larger spreading ranges it was not possible to prevent the formation of small layers during the filling of the tank. Therefore, the wider paths that form in the samples with larger distribution ranges are probably a result of flow through the layers and not of the distribution range. In the experiments with Baskarp sand, this layering is also a problem. It is not possible to prevent the formation of layers during filling due to the large grain size distribution range. Therefore, the experiments with Baskarp sand did not give reliable results.

In the experiments with grain size 149-250 micron no distinct preferential paths are visible in the steady state situation. There are a lot of small, braided paths that form one wide path of approximately 20 cm wide. When looking at the results of the 250-420 micron experiments, more distinct paths are visible, but they are still highly braided. The experiments with the 420-840 micron glass beads result in a couple of distinct preferential paths. These results imply that preferential flow paths become more distinct with increasing grain size or larger grain size distribution range.

The applied pressure has a significant influence on the flow of gas. Not only does the velocity of the gas increase if a higher pressure is applied, the width of spreading increases as well, with a maximum increase of width of 10 cm with a pressure increase of 10 mbar.

Considering breakthrough time, there is not an obvious relationship with grain size. In general it can be said that for a uniform sample, the breakthrough time lies within ten minutes of the start of the flow. Experiments conducted multiple times with the same grain size resulted in different breakthrough times. This is a result of the fact that each time the tank is filled, the grains are randomly distributed.

In some pictures paths where the gas was able to move the upper sand grains or glass beads were visible. The metal filter and weights placed upon them were not able to create a completely undeformable soil skeleton. This is probably the result of a small space between the glass plate and metal filter through which glass beads can move.
This particular problem will only occur under completely saturated conditions. When the top part is not saturated gas relative permeability of the gas phase is higher and there is no capillary pressure to overcome which will allow the gas to flow more easily through the grains.

Figures 6.14 - 6.17 clearly show that gas prefers to flow through a soil with the largest grain size and thus permeability. Gas will accumulate under less permeable layers until some kind of entry pressure is overcome and gas can flow through the less permeable layer. When accumulating under the less permeable layer, air was seen to spread over the whole length of

the tank in all experiments. This implies that if there is a less permeable layer situated in the soil, gas will accumulate under it and spread horizontally further than the 42 cm now observed.

From the experiment where the tank is filled with Baskarp sand with layers of 250-425 micron glass beads it can be seen that the ease with which the gas flows is also dependent on water pressure. When the gas is higher in the tank, the water pressure decreases and the flow rate of the gas increases.

In a completely saturated soil preferential paths will occur in soils with varying grain size. More distinct preferential paths can possible be expected in uniforms soils with a larger average grain size.
When a saturated soil is composed of a uniform sand without layering, a prediction can be made about the width of the spreading. This width seems to be independent on grain size. As soon as there is layering within the soil, the spreading width is dependent on the length of these layers. Because a larger grain size distribution range immediately results in layering and the spreading width of the gas will become wider. In these experiments perfectly rounded glass beads were used in which layering is more easily prevented than in sandy soils. This can be seen in the experiments with Baskarp sand. Even though Baskarp sand has a very steep grain size distribution (see Appendix A) layering still occurs. In a sandy soil with the same grain size distribution as the glass beads, even more layering is likely to occur and a larger spreading range is expected.
In the field layering of sand is thus very likely to occur. This makes it very difficult to make accurate predictions about the spreading width of the gas. A smaller grain size distribution range could result in more accurate predictions.

7. Discussion

7.1 Comparison between experimental and numerical work

In this section a comparison between the experimental and numerical results is made and the influence of different parameters, such as saturation and grain size, on the flow of gas through the subsurface is discussed.

From the small scale experiments it can be concluded that volumetric water content greatly influences the volumetric flow rate of gas measured at the surface. The volumetric flux measured at the surface at steady state conditions decreases with increasing degree of saturation. This is likely a result of a decreasing relative permeability of the gas.
Numerical simulations show a similar dependence. However, a much larger range between minimum and maximum values of volumetric flow rates exists in the experimental results compared to the numerical results. In the numerical simulations the maximum value for volumetric flux measured at the surface with a residual saturation is three times larger than the minimum value measured with a water level of 20 cm. In the experiments differences in volumetric flow rates of a factor of more than one hundred are measured between a completely dry soil and a soil with a water level of 8 cm above the gas inlet.
Differences between the numerical and experimental results are probably caused by a combination of the following phenomena:

- The simulations are conducted for equilibrium situations, whereas in the experiments probably no perfect equilibrium conditions occurred.
- The soil physical parameters used for the simulations are not the same as the parameters of the sand that is used for the experiments.
- As a result of the small scale of the experiments, water is pushed upwards in the column, creating a higher water pressure.
- In the numerical model, it is not possible to insert water pressure as a result of a water layer, because this is a one phase phenomenon. Simulations are conducted using a two-phase flow model in which other physical laws apply. However this water pressure is present in the experiments.
- In the experiment, porosity of the dry sample is higher than porosity of the saturated sample, whereas in the numerical model porosity is the same in both cases.

Both the experimental set-up and the numerical model should be improved for more quantitative results.

The one-dimensional column experiments suggest that flow of gas can also be prevented if the capillary pressure and water pressure are higher than the gas pressure. There seems to be a relation between breakthrough and grain size; breakthrough of natural gas occurs at a higher water level in a sample with a larger d_{15}. This is also in concurrence with the theory (Fetter, 1999) that states that soils with a smaller grain size have a larger entry pressure.
Theoretically, the entry pressure of a Dutch soil is approximately 0-30 kPa depending on the soil type (figure 5.1 Wörsten et al., 2001). This indicates that when there is a gas pressure of

100 mbar, no flow will occur when the water level is 70 cm above the pipeline. Due to the reduced relative gas permeability, volumetric fluxes measured at the surface will then be extremely small (in the range of ml/h). However, the 1-D column experiments indicate that the gas flow is prevented at much lower water levels for even larger grain sizes. This could be a result of the small scale of the setting, due to which water is pushed upwards in the column. It could also be a result of micro heterogeneities in the soil, which create a low permeability layer and prevent low.
Since in the numerical model the Van Genuchten parameters are used, no entry pressure is present. As discussed in Section 5.3.4.2, water pressure as a result of a layer of water cannot be included in the model, as a result flow will always occur in the simulations. It can be assumed that the numerical simulations will give a worst-case scenario, with highest possible flow rates of the gas.

The two-dimensional flow path experiments clearly show the existence of preferential flow paths in a saturated soil with varying grain size. The paths become more distinct with an increase in grain size. If there is no layering in the sample the total width of spreading seems to be independent of grain size and the occurrence of preferential path does not seem to cause a wider or narrower spreading range of the gas.
Contrary to the experiments, no distinct preferential paths are visible in the numerical simulations. This could be a result of the large size of the grid. When a grid size of a few millimeters is used, different results are expected.
Differences in soil stiffness between numerical simulations and field or laboratory experiments could also be a reason for the different results. In the numerical model complete soil stiffness is assumed. For low stiffness of the soil skeleton, an increase in gas pressure could result in substantially higher porosities than the initial value. Soil intrinsic permeability changes fast with porosity and therefore gas flow rates could increase rapidly. The influence of soil stiffness has also been suggested by Delahey and Alonso (2002).

Contrary to the experiments, the numerical simulations do indicate a change of spreading width with grain size. The simulations show an increase in spreading width with increasing grain size. At a residual saturation a medium grain size can have a maximum spreading width of 4 meters from the leakage, a very fine sand result in a maximum spreading width of 1.5 meters from the leakage. The difference between the numerical and experimental results could be a result of the small scale of the experimental setting and the fact that the experiments are conducted in a completely saturated soil, which results in a very low relative permeability of the gas.
The numerical simulations are more likely to show a realistic correlation. Therefore, spreading width is assumed to be dependent on grain size.
Since absolute permeability increases with increasing grain size, volumetric fluxes measured at the surface increase with increasing grain size as well.

The spreading width seems to depend on the applied gas pressure. The experiments as well as the numerical simulations show an increase of spreading width with increasing gas pressure. The numerical simulations show an increase in spreading width from the leakage from 2

meters, at a gas pressure of 30 mbar, to a spreading width of 3.5 meters from the leakage at a gas pressure of 100 mbar. A smaller pressure also leads to a smaller volumetric flux measured at the surface. The volumetric flux of gas measured at the surface is ten times larger when the gas pressure is 100 mbar compared to a gas pressure of 30 mbar. A possible correlation between gas pressure and spreading width for a soil could be determined if more simulations with different pressures are conducted.

The size of the leakage does not seem to have any influence on the total spreading width of the gas. An increase in size of the leakage does however cause an increase in volumetric flux of gas measured at the surface and causes a steeper concentration gradient of gas in the subsurface.

An important result from both numerical simulations and laboratory experiments is that layers of high permeability can result in spreading of gas through a high permeability layer. This can result in an increase in horizontal spreading width of the gas. In the experiments layering occurs mainly in the samples with a large variation in grain size distribution such as Baskarp sand. A large grain size distribution could thus lead to a large spreading width of the gas. However compared to natural sand Baskarp sand has a very steep grain size distribution curve. In the field layering of sand is thus even more likely to occur. This makes it very difficult to make accurate predictions about the spreading width of the gas. A smaller grain size distribution could result in more accurate predictions of the horizontal spreading width of the gas.
Similar to a high permeability layer in the soil a low permeability layer on top of a soil can cause a very wide spreading of the gas in the subsurface. If the intrinsic permeability of the low permeability layer is more than 500 times smaller than the intrinsic permeability of the soil, the gas will spread beneath this layer until a high permeability opening is found. This is approximately the difference between fine and coarse sand.

Due to the occurrence of side effects as a result of the small scale of the setting, it is difficult to make any quantitative comparisons between the experiments and numerical simulations. However, some quantitative comparison about the spreading width can be made between the numerical model and some large scale gas migration experiments conducted by Brötzenberger et al. (1987).

An important difference between the experiments conducted by Bötzenberg et al. (1987) and the numerical simulations is that in the experiments gas is forced through the domain at a constant flow rate and in the numerical simulations a flow as a result of a constant pressure is used. Another difference is that they did not conduct any experiments in the unsaturated zone, but only used a dry soil. This is unfortunate because experiments and simulations conducted in this study show that degree of saturation has a large influence on the spreading of gas. Results by Brötzenberg et al. (1987) indicate that the total spreading width of the gas in a dry soil does not change much with increasing gas flux, but that gas concentrations measured at the surface do increase with increasing flow rate. The results also show a steeper concentration gradient in horizontal direction. This is in concurrence with the results of the

simulations, which show a similar spreading distance for low concentrations of gas, of approximately 4 meters, but a steeper concentration gradient for gas at the center of spreading.
As shown in numerical simulations conducted in this study, results of Brötzenberg et al. (1987) show that frost, which leads to a low permeability layer, will lead to an increase in spreading width of the gas through the subsurface.
Brötzenberger et al. (1987) have managed to simulate a rain shower of 11.3 mm in 4 hours in their large scale experimental set-up. Their results show that precipitation only affects the concentration gradient when looking at small concentrations, which leads to a temporal decrease in width of the spreading of the gas. In their simulations these effects disappear within 24 hours. Results may be different when the soil is initially saturated or unsaturated.

7.2 Implications on the detection of gas

The results of the numerical simulations and laboratory experiments show that the flux of gas measured at the surface highly depends on the degree of saturation in the soil. Under field conditions a high degree of saturation can lead to small fluxes of gas measured at the surface in the range of millilitres per hour, even when there is a leakage of considerable size. If the soil becomes less saturated with time, for example as a result of seasonal variations in water level or as a result of groundwater extraction, this leakage can lead to a larger volumetric flux of gas.
Because of the influence of saturation on the flow rate of gas, observation of small fluxes of natural gas in a soil with a high degree of saturation cannot just be assumed to be a result of a small leakage. With a change in degree of saturation, this same leakage could result in a considerable flux of gas, which might result in a safety hazard.

Surveillance of pipelines will thus give the best results in a completely dry soil. Unfortunately gas distribution pipelines in the Netherlands are generally located in unsaturated soils. The degree of saturation is mainly dependent on the groundwater level and soil type. In the field, assuming an average Dutch soil, a groundwater level up to approximately 3.5 meter below the surface is expected to influence the degree of saturation above a pipeline as a result of capillary rise (figure 5,1, Wörsten et al., 2001). This will then influence the volume flux of gas measured at the surface. Because the height to which capillary rise can influence the degree of saturation depends on the grain size of the soil, a smaller grain size results in a higher capillary rise (Fetter, 1999).
When the groundwater level is above the pipeline, this will also influence the migration of gas. If the sum of the water pressure and entry pressure of a soil is larger than the pressure in the pipeline, no flow of gas will occur. Depending on the d_{15} diameter of the soil, the entry pressure, the pressure in the pipeline and the water pressure it can be estimated if flow of gas will occur.

In this study, no results on the influence of precipitation on the flow of gas through the subsurface are obtained. Results from large scale experiments conducted by Brötzenberger et

al. (1987) indicate that a rain shower has no influence in the high concentration zones of the gas, but it has influence in low concentration zones, resulting in a decrease of total spreading width of the gas. These effects last approximately 24 hours. Detection of gas thus seems to be possible soon after a rain shower. However, a rain shower could have more influence in a partly saturated soil. This should be the subject of future studies.

As stated before, layering of different grain sizes results in a wider spreading of the gas. Natural gas will always flow through high permeability regions, and it will spread through a high permeable layer as far as this layer is continuous. Layering must thus be prevented when covering a pipeline with sand. Because layering is most likely to occur in soils with a broad grain size distribution, it is best to use a cover material with a small grain size variation. Layering due to a decreased porosity as a result of tamping of the cover material, will probably not have any influence on the spreading width of the gas. Calculations using maximum and minimum porosities of natural sand (Study Centre for Road Construction, 1978) and assuming minimum compaction of 50% , a decrease in porosity as a result of tamping will lead to a maximum decrease of 50% in permeability. Simulations described in Section 5.3.6 have shown that accumulation under a low permeability layer will only occur when the permeability of the covering layer is more than 10 times as small as the permeability of the subsurface.
Ice or other covering materials can lead to a low permeable layer on top of the soil. These layers can lead to an enhanced horizontal spreading of the gas beneath the low permeability layer. It will be very difficult to determine the exact location of the gas. Gas is most likely to flow through a high permeability hole or crack in a low permeability layer. Gas concentrations obtained during surveillance of pipelines can therefore give very distorted and vague information on the possible location of the leakage.

Because the flow of gas seems to be highly dependent on differences in permeability, it is likely that the flow is also influenced by other heterogeneities, such as cracks in the subsurface. These can be a result of natural causes, such as the growth of plants or can be caused by human activity. It is likely that these cracks give a path of high permeability. As a result of this high permeability path, the gas is likely to flow through these predetermined paths.

For surveillance purposes it will be very useful to have detailed knowledge of soil type, groundwater level and water content of the soil. Without this knowledge only a rough estimate can be made using the average parameters for Dutch soils. In a soil without layering, the width of spreading can range from approximately 1 to 3.5 m from the leakage. When layering is present, the spreading range can become much larger.

It can be useful if at all locations similar soils are used to cover the pipelines. As stated above, without knowledge of the soil type it is very difficult to say anything useful about the distribution of the gas in the soil. A cover material consisting of a medium to coarse sand with small range in grain size is preferred. Such a soil will have a high intrinsic permeability. As long as the intrinsic permeability of the cover material is larger than the intrinsic permeability

of the surrounding soil, gas will only spread through the cover material. The spreading width in the direction of the pipeline will be up to 1 meter larger when a coarse sand instead of a fine sand is used. The influence of saturation as a result of capillary rise is also limited when coarser sand is used. Because of the high intrinsic permeability the infiltration rate of precipitation will be faster. This results in a limited influence of precipitation.
Because of the large intrinsic permeability, average volume fluxes of natural gas will also be larger at the surface. This leads to higher concentrations of natural gas in the air, which are easier to detect. A disadvantage could be that these higher gas concentrations can lead to a safety hazard.
If flow of gas is to be prevented or smaller fluxes of gas are more desired, it would be a better idea to use a very low permeable soil. Due to high capillary pressure it is more likely that flow of gas through the soil is prevented. Due to the lower intrinsic permeability, smaller volume fluxes will be observed. However, the flow of gas through this soil type will be very hard to predict and accumulation of gas is more likely to occur, which can also result in a safety hazard. To get a better idea of the advantages and disadvantages of different sands, more research is recommended.

7.3 Recommendations for further research

In the 1-D column experiments conducted in this study, boundary effects caused by the limited size of the setting, are expected to greatly influence the results. If experimental work will be continued, it will be very useful to conduct some large scale three dimensional experiments to simulate all the processes at their actual scale. These experiments could be similar to the ones executed by Brötzenberger et al. (1987). Depending on the soil type and applied pressure used, the size of such a set-up must be approximately 10 meter in length and width and at least 80 cm high. The main point of improvement of the experiments compared to the experiments done by Brötzenberger et al. (1987) is that degree of saturation must also be studied and that gas must flow in as a result of a pressure difference instead of a constant flux. Such an experiment will however be very hard to conduct. It will be necessary to have complete knowledge of the degree of saturation in the set-up. This was already a problem in the small setting and will be very difficult in a larger set-up. Because the placement of TDR's will be difficult, perhaps the volumetric water content can be measured with some sort of γ-ray attenuation system as used in Tyner et al. (2005). Extraction of the water from the bottom could also be problematic in a large scale set-up, because extraction from different points can cause preferential paths with a low degree of saturation. It would be useful to conduct several experiments using different grain sizes. Just as the experiments described above, it will be very time-consuming experiments as a new set-up has to be created every time gas has flown through the sample. Of course the expenses for such an experiment would also be considerable.
However, such an experiment could result in quantitative results for volumetric fluxes of gas measured at the surface and spreading width of the gas for different soil types and water levels which will be similar to values that can be expected in the field. In a smaller setting

side effects are likely to occur which can influence the pressure and saturation distributions resulting in distorted results.

A number of improvements can also be made to the numerical simulations. First it would be very good if three-dimensional simulations could be conducted. Although the processes are the same, more realistic quantitative values for fluxes of gas flowing out of the domain could then be given. Because three-dimensional simulation would require much more grid cells, simulations will require a very long calculation time, especially when a random permeability is implemented on the nodes. Seeing that the two-dimensional model already required parallel computation of up to two days using 8 processors at SARA, the calculation time for a three dimensional simulation can be considerable. The program should be optimized to conduct three-dimensional simulations.
It would also be useful if the numerical model could accurately simulate small scale experiments. Right now, distortions occur at the boundaries, which eventually cause the discretization to diverge.
A main point of improvement is to create the possibility for the program to change from a one-phase flow system to a two-phase flow system. This is the so-called multiphysics. As has been discussed in Chapter 5.3, this is a very complex problem because of the completely different physical processes that occur in one and a two-phase systems. Because of the complexity of such a task, this goes beyond the scope of a six months MSc-project and is more in the scope of a PhD-project.

A combination of large scale experiments with different degrees of saturation and improved numerical modelling would greatly enhance the understanding of gas migration through the unsaturated soil. This would allow for a model calibration to be made and the model then permits extensions to field conditions. This would be very useful to anticipate any problems that might occur in the field.

8. Conclusions

Migration of natural gas through the soil as a result of a leakage is dependent on a number of physical parameters. The combination of these different parameters determines the migration of gas through the subsurface.

Degree of saturation has a large influence on the spreading width of natural gas. In a fine sand a water level that is 20 cm above the leakage results in a spreading width of 1.8 meters, whereas a residual water saturation results in a spreading width of 3 meters. An increasing saturation results in a decreasing gas permeability. As a result, the volumetric gas flux measured at the surface is 3-100 times larger at residual saturation than at a water level of 20 cm above the leakage. For an average Dutch soil, a water level of 3.5 meter below the surface can influence the saturation in the upper 80 cm of the soil.
Soil type also influences the migration of gas. A smaller grain size results in a smaller spreading width and volumetric flux measured at the surface. The difference in maximum spreading width between clay and fine sand is approximately 1.5-2.0 meters. The difference between fine and coarse sand is approximately 0.5-1.0 meter.
A larger pressure in the pipelines will cause an increase in spreading width and volumetric flux. For a pressure of 100 mbar and water level at the height of the leakage, spreading width is 3.5 meters for a medium sand, whereas for a pressure of 30 mbar under the same conditions, the spreading width is 2 meters. The volumetric flux at the surface is about 10 times higher with a pressure of 100 mbar than with a pressure of 30 mbar.
Broad grain size distributions cause layering of a soil due to sedimentation effects. Because natural gas will preferably flow through high permeability zones, these zones result in a very wide spreading range of the gas. To prevent wide spreading as a result of broad grain size distributions, it is useful to use a sand with a small grain size distribution to cover the pipelines. If a sand with considerable coarser grains than the surrounding soil is used to cover the pipelines, natural gas will only flow through the coarse sand and spreading width can be reduced considerably. This results in an easier detection of leakages.
Low permeability layers on top of a soil can also cause a wide horizontal spreading of natural gas under this low permeability layer. If the intrinsic permeability of the low permeability layer is more than 500 times smaller than the intrinsic permeability of the soil, the gas will spread beneath this layer until a high permeability opening is found. This is approximately the difference between fine and coarse sand. This implies that it is very difficult to determine the exact location of a leakage when a cover material – like ice or pavement – is present.

Precipitation does not seem to have a significant effect on the flow of gas in dry porous media. The influence of precipitation on unsaturated or partly saturated media has to be investigated in further studies.

The knowledge of the flow of gas through an unsaturated soil is still limited and further research is definitely necessary. The combination of large scale experiments with different degrees of saturation and improved numerical modeling would greatly enhance our understanding of gas migration through the unsaturated soil. This will also allow for model

calibrations, the model then permits extensions to field conditions. This would be very useful to anticipate to any problem that might occur in the field.

9. Acknowledgements

First of all we would like to thank our supervisor Prof. Dr. Ruud Schotting of the University of Utrecht for providing guidance during the research and for reviewing our work.

We would like to thank Deltares for giving us the opportunity to conduct experiments in their facilities and for the opportunity to get to know the company. At Deltares we would especially like to thank our supervisors Dr. Adam Bezuijen, Ir. Paul Schaminée and Ir. Vera van Beek for guidance during the entire project reviewing our work. We would like to thank Thijs van Dijk for constructing the experimental set-up and adjusting it when necessary. Ferry Schenkeveld is thanked for his help during the experiments, when he was always there to help us out.

Thanks also goes out to Dr. Kees Pulles and ir. Youri van der Drift from KIWA Gas Technology for providing information on gas leakages and for reviewing our work.

We would also like to thank everyone in the department of Hydromechanics and Hydrosystem modeling at the University of Stuttgart for helping us getting started with MUFTE-UG. Our special thanks goes out to Dr. Jennifer Niessner, who we could always bother if we had any questions during her stay in Utrecht.

We also want to express our gratitude to Theo van Zessen from the University of Utrecht who has always helped us if we had any problems with the installation of our computer and program. And finally we would like to thank Thomas Geenen for making it possible to run our model at SARA.

10. References

Assteerawatt, N., Bastian, P., Bielinski, A., Breiting, T., Class, H., Ebigbo, A., Eichel, H., Freiboth, S., Helmig, R., Kopp, A., Niessner, J., Ochs, S., Papafotiou, A., Paul, M., Sheta, H., Werner, D., Ölmann, U. (2005) MUFTE-UG: Structure, Applications andNumerical Methods. Newsletter, International Groundwater Modeling Centre, Colorado School of Mine, 10/2005. - Volume XXIII ISSUE 2

Bastian, P., and Helmig, R. (1999) Efficient Fully-Coupled Solution Techniques. Two Phase Flow in Porous Media. Parallel Multigrid Solution and Computations. Advances in Water Resources, 23:199 – 216.

Bear, J. (1972) Dynamics of fluids in porous media, Elsevier, New York.

Bear, J. (1979) Hydraulics of groundwater. McGraw-Hill, New York.

Bohne, K., & Nitsche, C. (1992) Requirements and use of indirect methods for estimating the hydraulic functions of unsaturated soils. In: van Genuchten, M. Th., F. J. Leij, and L. J. Lund (eds.), Proc. Int. Workshop, Indirect Methods for Estimating the Hydraulic Properties of Unsaturated Soils. pp. 359-368, University of California, Riverside.

Brooks, R. H., and Corey, A.T. (1964) Hydraulic properties of porous media. Hydrol. Pap., volume 3. Fort Collins, Colorado State University.

Brötzenberger, H., and Pass, F. (1987) Untersuchungen zur Ausbreitung von Erdgas im Boden, gwf Das Gas- und Wasserfach, Gas – Erdgas, vol. 128 nr. 2 pp. 69-77

Burdine, N.T. (1953) Relative permeability calculations from pore-size distribution data. Technical report, Petroleum transactions of the AIME.

Conciani, W., Soares, M.M., Crestana, S., 1995. Geotechnical use of mini tomography. UNSAT'95. In: Alonso, E.E., Delage, P. (Eds.), Proc. First Int. Conf. On Unsat. Soils. Unsaturated Soils, vol. 2. Balkema.

Delahaye, C.H., & Alonso, E. E. (2002) Soil heterogeneity and preferential paths for gas migration. Engineering Geology vol. 64, pp. 251–271

Dogan, M.O.(2004) Modeling of mine gas repositories. Msc thesis, Institüt für Wasserbau, Universität Stuttgart.

Fetter, C.W. (1999) Contaminant hydrogeology. Second Edition. Prentice Hall, Inc. New Jersey.

Fitts, C. R. (2002) Groundwater science. Academic Press, San Diego, CA.

Genuchten van, M.T. (1980) A closed-form equation for predicting the hydraulic conductivity of unsaturated soils. Soil Sci. Soc. Am. J., vol 44, pp 892-898.

Günzel, F. K., Craig, W., H., Cranon, P., Cottineau, L. M., Kechavarzi, C., Lynch, R. J., Merrifield, C. M., Oung, O., Schenkeveld, F., Soga, K., Thorel, L., & Weststrate, A. (2003) Evaluation of probes and techniques for water content monitoring in geotechnical centrifuge models. International journal of physical modeling in geotechniques, vol. 1, pp. 21-43.

Helmig, R. (1997) Multiphase flow and transport processes in the subsurface. A contribution to the modeling of hydrosystems. Springer – verlag Berlin Heidelberg New York.

Helmig, R., Class, H., Huber, R., Sheta, H., Ewing, R., Hinkelmann, R., Jakobs, H., and Bastian, P. (1998) Architecture of the Modular Program System MUFTE UG for Simulating Multiphase Flow and Transport Processes in Heterogeneous Porous Media. Mathematische Geologie, 2, 123-131.

Hillel, D. (2004) Environmental soil physics. Academic press.

Iwata, T., Hamaide, G., and Fuchimoto, K.(1992) Development of analytical methods for the behaviour of underground leakage gas from low-pressure mains. Proceedings of the International Gas Research Conference.

Manthey, S. (2006) Two-phase flow processes with dynamic effects in porous media – parameter estimation and simulation. PhD-thesis, Institut für Wasserbau der Universität Stuttgart.

Metcalfe, D. E., & Farquhar, G. J. (1987) Modeling gas migration through unsaturated soils from waste disposal sites. Water, air and soil pollution, volume 32, nr 1-2.

Mualem, Y. (1976) A new model for predicting the hydraulic conductivity of unsaturated porous media. Water resources research, vol. 12, pp. 513-522.

Poel, van der, J. T., & Schenkeveld, F. (1998) A preparation technique for very homogenous sand models and CPT research, Centrifuge 98, pp 149-154.

Study Centre for Road Construction (1978) Various properties of natural sand for Netherlands highway engineering, Arnhem.

Wörsten, J. H. M., Veerman, G. H., de Groot, W. J. M., & Stolte, J. (2001) Waterretentie en doorlatingskarakteristieken van boven- en ondergronden in Nederland: de Staringreeks. Vernieuwde uitgave 2001. Alterra report 153. Alterra, Research Instituut voor de Groene Ruimte, Wageningen.

Appendix A

Grain size distribution diagram of Baskarp sand (geosfeer.geodelft.nl, Geodelft).

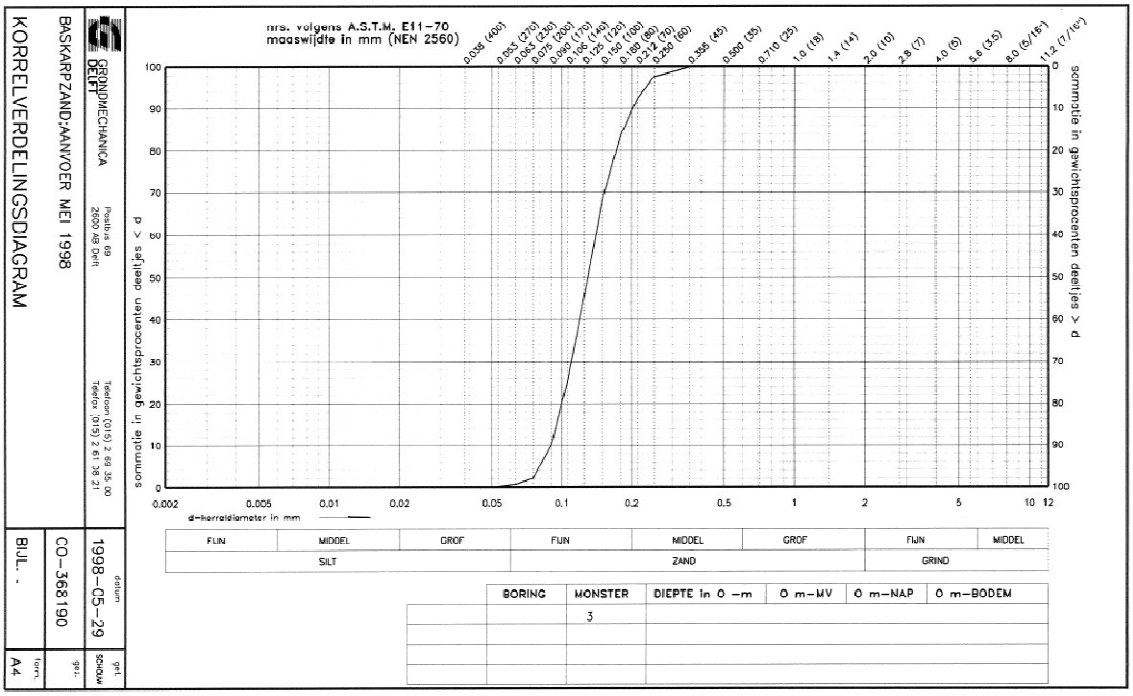

List of figures

Chapter 6

List of tables

Chapter 5

Chapter 6